JGR Atmospheres

Special Section:
Understanding carbon-climate feedbacks

Key Points:
- The elevated atmospheric CO_2 had a strong positive influence on gross primary productivity (GPP) and also offset deforestation, when native forest was converted to grasses
- Land use change also had a negative effect on evaporation and most intense effects of climate change (as temperature increasing) were on deforested areas
- Uncertainties were found in the outputs of the models and in the climatic forcings. Divergences were also observed among the models

Supporting Information:
Supporting Information may be found in the online version of this article.

Correspondence to:
L. F. C. Rezende,
luizfeliperezende@gmail.com

Author Contributions:
Conceptualization: Luiz F. C. Rezende, Celso Von Randow
Data curation: Luiz F. C. Rezende, Aline Anderson de Castro, Romina Ruscica, Boris Sakschewski, Phillip Papastefanou, Nicolas Viovy
Formal analysis: Luiz F. C. Rezende
Funding acquisition: Celso Von Randow, Kirsten Thonicke, Anja Rammig, Iracema F. A. Cavalcanti

Impacts of Land Use Change and Atmospheric CO₂ on Gross Primary Productivity (GPP), Evaporation, and Climate in Southern Amazon

Luiz F. C. Rezende[1] , **Aline Anderson de Castro[1]**, **Celso Von Randow[1]** , **Romina Ruscica[2,3,4]** ,
Boris Sakschewski[5], **Phillip Papastefanou[6]** , **Nicolas Viovy[7]** , **Kirsten Thonicke[5]** ,
Anna Sörensson[2,3,4] , **Anja Rammig[6]** , and **Iracema F. A. Cavalcanti[1]**

[1]National Institute for Space Research (INPE), São José dos Campos, Brazil, [2]Facultad de Ciencias Exactas y Naturales, Universidad de Buenos Aires, Buenos Aires, Argentina, [3]CONICET – Universidad de Buenos Aires, Centro de Investigaciones del Mar y la Atmósfera (CIMA), Buenos Aires, Argentina, [4]CNRS – IRD – CONICET – UBA, Instituto Franco-Argentino para el Estudio del Clima y sus Impactos (UMI 3351 IFAECI), Buenos Aires, Argentina, [5]Potsdam Institute for Climate Impact Research (PIK), Potsdam, Germany, [6]Technical University of Munich (TUM), Munich, Germany, [7]Le Laboratoire des Sciences du Climat et de l'Environnement (LSCE), Gif sur Yvette, France

Abstract Recent publications indicate that the Amazon may be acting more as a carbon source than a sink in some regions. Moreover, the Amazon is a source of moisture for other regions in the continent, and deforestation over the years may be reducing this function. In this work, we analyze the impacts of elevated CO_2 (eCO_2) and land use change (LUC) on gross primary productivity (GPP) and evaporation in the southern Amazon (7°S 14°S, 66°W 51°W), which suffered strong anthropogenic influence in the period of 1981–2010. We ran four dynamic global vegetation models (DGVMs), isolating historical CO_2, constant CO_2, LUC, and potential natural vegetation scenarios with three climate variable data sets: precipitation, temperature, and shortwave radiation. We compared the outputs to five "observational" data sets obtained through eddy covariance, remote sensing, meteorological measurements, and machine learning. The results indicate that eCO_2 may have offset deforestation, with GPP increasing by ~13.5% and 9.3% (dry and rainy seasons, respectively). After isolating the LUC effect, a reduction in evaporation of ~4% and ~1.2% (dry and rainy seasons, respectively) was observed. The analysis of forcings in subregions under strong anthropogenic impact revealed a reduction in precipitation of ~15 and 30 mm, and a temperature rise of 1°C and 0.6°C (dry and rainy seasons, respectively). Differences in the implementation of plant physiology and leaf area index in the DGVMs introduced some uncertainties in the interpretation of the results. Nevertheless, we consider that it was an important exercise given the relevance.

1. Introduction

The Amazon rainforest is currently suffering two major impacts: climate change and deforestation, with land use change (LUC) in Brazil both driving climate change at local and regional scales and being susceptible to global climate changes (Lapola et al., 2014). LUC extended massively from 1990 to 2011 pushed by governmental infrastructure investment programs, such as road expansion (D. S. Alves, 2002). Deforestation near roads is a recurring pattern, and D. S. Alves (2002) estimated that around 90% of deforestation from 1991 to 1997 was at a distance of up to 100 km from main roads built in the framework of government development programs. Additional factors stimulated agricultural expansion, such as energy supply facilities and low land prices (Lapola et al., 2014; Leite et al., 2011; Leite-Filho et al., 2019). Pastures and cropland areas increased from 26,115 km² in 1998 to 56,138 km² in 2012 (Dias et al., 2016; Leite-Filho et al., 2019). Most of the deforested area (60%–80%) is used for pastures for livestock (Lapola et al., 2014), although the sequence of land uses following deforestation is spatially heterogeneous (Muller-Hansen et al., 2017). Concerted action of new law enforcement aimed at combating illegal deforestation, reducing the use of fire in the deforestation process, and increasing the size of protected areas, with the contribution of soybean and cattle moratoria have greatly reduced annual deforestation between 2011 and 2015 (INPE-Prodes, 2020; Nepstad et al., 2014). Moreover, it led to the policy incentive to achieve zero deforestation by 2020 (Aguiar et al., 2016; Azevedo et al., 2017). Beyond the use of fire for deforestation, the analysis of anthropogenic forest disturbances including selective logging, reveals an urgent need for policy interventions that go beyond maintaining the forest cover (Barlow et al., 2016).

Methodology: Luiz F. C. Rezende, Aline Anderson de Castro, Celso Von Randow, Iracema F. A. Cavalcanti
Project Administration: Kirsten Thonicke, Anja Rammig, Iracema F. A. Cavalcanti
Software: Luiz F. C. Rezende, Aline Anderson de Castro, Boris Sakschewski, Phillip Papastefanou, Nicolas Viovy
Supervision: Celso Von Randow, Iracema F. A. Cavalcanti
Validation: Luiz F. C. Rezende
Visualization: Luiz F. C. Rezende
Writing – original draft: Luiz F. C. Rezende
Writing – review & editing: Aline Anderson de Castro, Romina Ruscica, Boris Sakschewski, Phillip Papastefanou, Nicolas Viovy, Kirsten Thonicke, Anna Sörensson, Anja Rammig, Iracema F. A. Cavalcanti

Deforestation and its impacts on climate have been studied for some time and in general, researchers agree that temperature is rising and evaporation is decreasing (Llopart et al., 2018; Nobre et al., 1991; Sampaio et al., 2007). In this manuscript, we use the term evaporation with the commonly accepted meaning of evapotranspiration, following Miralles et al. (2020) who argue that it is more appropriate to describe evaporation as the sum of three processes: transpiration which is the evaporation of water from vegetation that occurs through stomata, loss by interception which is the evaporation of rainwater intercepted by the canopy, and evaporation of soil water.

Evaporation in the Amazon has strong climate implications with moisture contributing 25%–70% of the precipitation in southeastern South America (Dirmeyer et al., 2009; Sörensson & Ruscica, 2018; van der Ent et al., 2010; Zemp et al., 2014). Still, evaporation over the Amazon region at the end of the dry season contributes to triggering the onset of the South American Monsoon System, which suggests the existence of intrinsic interactions between tropical forest phenology and climate (Li & Fu, 2004; Sörensson & Ruscia, 2018; Wu et al., 2016). Changes in the land surface may also affect the cycles of energy, water, carbon, trace gases, and nutrients in the region (Avissar et al., 2002; Barlow et al., 2007; Cardille & Foley, 2003; Silva Dias et al., 2002; C. Von Randow et al., 2004; R. C. S. Von Randow et al., 2020). That interaction was a key research theme of the Large-Scale Amazon Biosphere-Atmosphere Experiment (LBA). Other LUC aspects, such as logging and small-scale disturbances are also responsible for biodiversity loss in the Amazon region, as they contribute to further degrade tropical forests (Barlow et al., 2016, 2018; Intergovernmental Panel on Climate Change, 2019).

Furthermore, the Amazon rainforest is an important sink and reservoir for carbon (Brienen et al., 2015; Pan et al., 2011). Estimates based on forest inventories in the Amazon basin showed that undisturbed tropical forests act as a strong carbon sink with an estimated annual uptake of 0.42–0.65 PgCyr^{-1} for 1990–2007, around 25% of the residual terrestrial carbon sink (Brienen et al., 2015). This sink is probably driven by increasing atmospheric CO_2 via the downstream effects of increased photosynthesis (fertilization) and intrinsic water use efficiency (WUE; Fleischer et al., 2019; Ueyama et al., 2020; Walker et al., 2020). The sink is particularly pronounced in the simulations of the response of tropical forests in dynamic vegetation models (Fleischer et al., 2019) and has substantial uncertainties because there is no empirical evidence for the CO_2 response in the tropics (e.g., Norby et al., 2015). On the other hand, using various satellite and ground-based data sets for the period 1982–2015, Wang et al. (2020) showed that global carbon sequestration decreased in most land regions of the globe. This decrease was well correlated with changes in nutrient concentrations in vegetation (N and P) and the availability of water in the soil. Gatti et al. (2021) observed that regions under greater anthropogenic influence, such as the southeast of the Amazon, have acted more as a carbon source than a sink. Another contribution to uncertainty is that models have weaknesses in representing the relationships between net productivity and biomass (Dolman & Janssen, 2018). In addition, carbon inventory observational data point toward a decline in carbon uptake in the Amazon, which might reach zero by 2035 (Hubau et al., 2020). The drivers for this decline might be increased mortality of biomass due to rising temperatures and drought stress, but also due to a faster turnover of biomass driven by increased CO_2 concentration (Hubau et al., 2020). Losing the Amazon carbon sink by deforestation and climate change would significantly intensify the climate crisis, as mature forests across the entire Amazon region have contributed significantly to mitigating climate change in the past decades (Phillips & Roel, 2017) photosynthetic process.

In our study, we compare and assess gross primary productivity (GPP) and evaporation modeled with four Dynamic Global Vegetation Models (INLAND, LPJ-GUESS, LPJmL4, and ORCHIDEE) using FLUXCOM data obtained from flux towers, remote sensing, and meteorological observations (Baldocchi et al., 2001; Jung et al., 2020), light use efficiency (LUE; Madani & Parazoo, 2020), Global Land Evaporation Amsterdam Model1,2 (GLEAM; Czikowsky & Fitzjarrald, 2009; Miralles et al., 2010), and TerraClimate—a data set of climate and water balance variables for global land surfaces. To examine the uncertainty in historical climate forcing data sets, we used three data sets as climate forcings (GLDAS 2.0, GSWP3, and WATCH + WFDEI) in the DGVMs. We also used these climate forcing sets as "observed data" to analyze changes in temperature and precipitation in the study region.

We seek here to understand and evaluate the impacts of LUC and increasing atmospheric CO_2 concentration on evaporation and carbon assimilation in the forests of the Amazon biome during 1981–2010. A specific objective is to evaluate which factor, LUC or eCO_2 affects (negatively or positively) the productivity (GPP) of the Amazon forests the most. In summary, we seek to study the impacts of increased atmospheric CO_2 and deforestation on GPP and evaporation in the Amazon knowing that this biome plays an important role in the climate of the region and the planet.
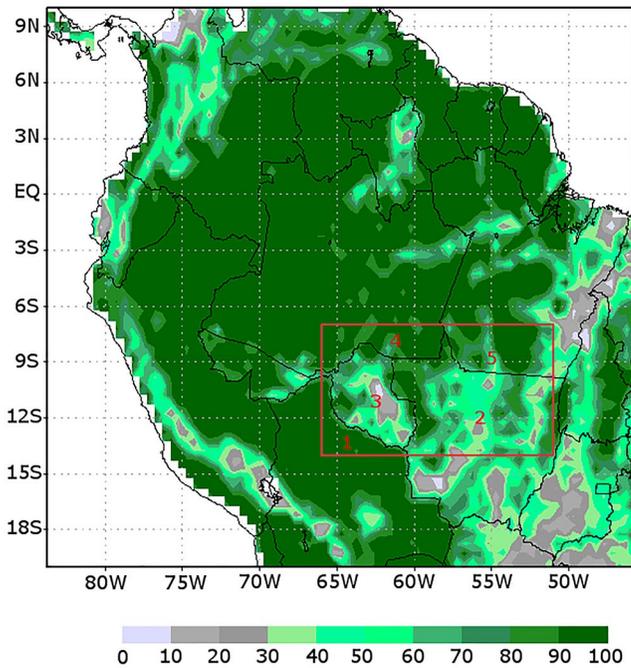
Figure 1. Vegetation cover (%), study region (rectangle red line): North of Bolivia (a); Brazil, states: northern Mato Grosso (b), Rondonia (c), southern Amazonas (d) and southern Pará (e).

2. Data and Methods

2.1. Study Region and Definition of Seasons

Although the simulations were done for the whole of South America, we delimited our study area in the southern Amazon between 7°S and 14°S of latitude and 66°W and 51°W of longitude (Figure 1), as this region has been one of the most affected by deforestation and LUC in the past 30 yr (Kalamandeen et al., 2018; Leite-Filho et al., 2019). The region comprises the states of Rondônia, southern Amazonia, northern Mato Grosso, and southern Pará in Brazil; and the northern part of Bolivia.

Much of the Bolivian territory included in our study consists of wetlands. However, significant land cover change has taken place in the north of that country near the border with Brazil (Tejada et al., 2016). Indeed, extensive areas were deforested for soybean cultivation and cattle ranching in the Bolivian Amazon in the mid-1980s (Kileen et al., 2007; Tejada et al., 2016).

Because of its large area, the Amazon basin has different climate regimes. Thus, we adopted the methodology applied by Alves et al. (2013) for the south of our study region. We defined the rainy season to include the months with the greatest precipitation (January, February, March, and April—JFMA) and the dry season, the months of lower precipitation (June, July, August, and September—JJAS).

2.2. Models, Data Set, and Conditions of Simulations

We used four models that are classified as dynamic global vegetation models (DGVMs; Prentice et al., 2007; Rezende et al., 2015): INLAND (Tourigny, 2014); LPJmL4 (Schaphoff et al., 2018), LPJ-GUESS (Hickler et al., 2012; B. Smith et al., 2001), and ORCHIDEE (Krinner et al., 2005). DGVMs are powerful tools to project past, present, and future vegetation patterns and associated biogeochemical cycles in global scale studies (Quillet et al., 2009; Scheiter et al., 2013). DGVMs simulate surface processes such as the transfer of energy, water, and momentum between the land surface and the atmosphere, as well as biogeochemical cycles, carbon assimilation by vegetation, phenology, and vegetation growth and mortality. This type of model is becoming increasingly able to simulate land use changes (Prentice et al., 2007; Rezende et al., 2015).

2.2.1. Climate Forcing Data Sets and Simulation Conditions

Forcing data from the following sources were used: GLDAS 2.0—Global Land Data Assimilation System (GLDAS; https://ldas.gsfc.nasa.gov/gldas; Rodel et al., 2004); GSWP3—Global Soil Wetness Project Phase 3 (GSWP3; http://hydro.iis.u-tokyo.ac.jp/GSWP3/; Kim, 2017); and WATCH + WFDEI (https://www.isimip.org/gettingstarted/details/5/; Weedon et al., 2014, 2011). All data sets have daily temporal resolution and spatial resolution of 0.5° × 0.5°.

We conducted two sets of simulation experiments with different values of CO_2: (a) increasing CO_2 from the pre-industrial period to 2010 named historical CO_2 (hist CO_2); (b) constant concentration of 278 ppm of (pre-industrial) atmospheric CO_2 named constant CO_2 (const CO_2). We ran both CO_2 experiments under LUC and potential natural vegetation (PNV) conditions, respectively (Chiarucci et al., 2010; Leipprand & Gerten, 2006). In the PNV experiments, vegetation dynamics are the result of climate and soil conditions without anthropogenic influence. All combinations of CO_2 and land cover change resulted in four sets of simulation experiments per climate input: 1. LUC historical CO_2; 2. LUC constant CO_2; 3. PNV historical CO_2; 4. PNV constant CO_2. For each set of simulation experiments, all three climate input data sets were applied; therefore, we obtained twelve (3 × 4) simulations per model (Figure 2). Before conducting the described set of simulations, the DGVMs were first run with spin-ups ranging from 1,000 to 2,000 yr to achieve equilibrium between climate and the respective vegetation and soil carbon pools following the same simulation protocol. After the spin-up, the DGVMs were run from 1950, although the period under study was 1981–2010. The simulations were performed throughout South America, although our study area is restricted to the southern Amazon, as described in Section 2.1.
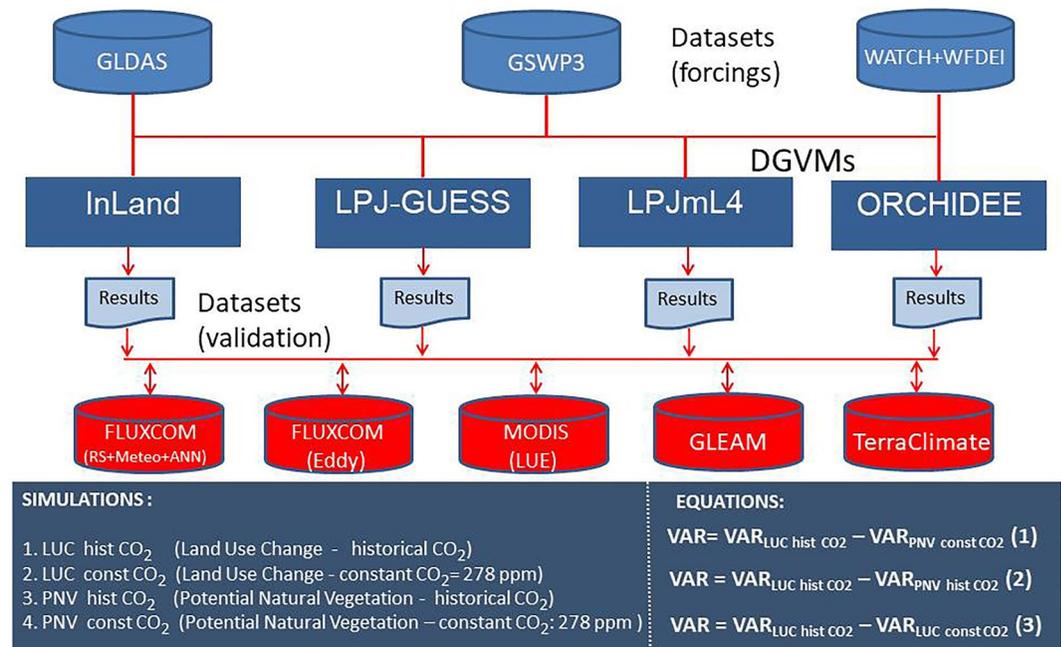
Figure 2. Diagram and scheme of the experiment: atmospheric data set used (forcings), dynamic global vegetation models (DGVMs), DGVM results, data sets for validation, conditions of simulations, and effect-isolating equations.

2.2.2. LUC Data Set and PNV

LUC data were based on a composition of PRODES Amazônia (http://www.obt.inpe.br/OBT/assuntos/progra-mas/amazonia/prodes) for the Brazilian Amazon and LUH2 (Land Use Harmonization, http://luh.umd.edu/) for the other South American countries (Hurtt et al., 2020). PRODES is a project developed at INPE (National Institute for Spatial Research; INPE-PRODES, 2020) to monitor vegetation clear-cutting using satellite data. The LUH2 is a set of data that connects a historical reconstruction of land use (based on HYDE—History Database of the Global Environment) to future projections. Because PRODES data is only available from 2002, LUH2 data were interpolated from 1980 to 2002, to fit the PRODES data period. In the INLAND model, land-cover change is represented by a tiling approach where each grid cell is divided into two tiles, one representing the fraction of natural vegetation and the other one representing the fraction of anthropogenic (deforested or managed) land at each grid cell, from land use maps. The first tile simulates dynamic natural vegetation that is altered according to the yearly carbon inflow and outflow, and the second one simulates a prescribed grassland that is used to represent anthropogenic land. The final fluxes and stocks of each grid cell are calculated by the average of the two tiles, weighted by the fraction of each tile.

We adopted here the term PNV, but we are aware that this approach has been criticized for its unrealism in dealing with ecosystem dynamics, as biological processes such as senescence, growth, and mortality are treated without considering anthropogenic interference (Chiarucci et al., 2010). It is also important to note that each of the DGVMs we used in this experiment has its own way of dealing with these and other issues related to plant physiology, as we discuss in more detail in Section 4.1. In addition, we assume that the PNV is correct from 1950, the year when our simulations started (after the spin-up), although the period analyzed was from 1981 to 2010. We also warn that LUC may be slightly overestimated by this procedure.

2.2.3. Data Sets for Validation

We used the following data sets for validation:

1. GPP and evaporation from FLUXCOM (Jung et al., 2020; Figure 1) were used to evaluate DGVM results (Figure 2). Part of the FLUXCOM data were obtained by the FLUXNET initiative which provides estimates of carbon flows between the biosphere and atmosphere based on globally distributed eddy covariance flux towers (Baldocchi et al., 2001; Jung et al., 2020). As flux towers have a small footprint and are distributed

unevenly across the world, the upscaling approach is based on machine learning methods (artificial neural networks) that integrate FLUXNET site-level observations (eddy covariance measurements), remotely sensed data (fluxes estimated from mean seasonal cycles of Moderate Resolution Imaging Spectroradiometer—with techniques of Sun-Induced Fluorescence and atmospheric inversion results), and meteorological data (daily meteorological information; Jung et al., 2020). We used the following versions of FLUXCOM data sets: GPP ANN CRUNCEP version 6 (for GPP), and LE.METEO.EBC.MLM.CRUNCEP version 8 (for evaporation); both provided at monthly resolution. Information about FLUXCOM and downloading instructions can be found at http://www.fluxcom.org/ (accessed on 20 November 2020)

2. Derived GPP by upscaling observations from the current global network of eddy covariance towers (Jung et al., 2020). Eddy covariance measurements are processed half-hourly using standardized procedures of gap filling and quality control (Moffat et al., 2007; Papale et al., 2006). Data are subsequently aggregated into monthly means, which reduces random errors. Monthly means having over 20% data based on low-confidence gap filling are excluded from the analysis to minimize uncertainties (Reichstein et al., 2005). For this data set, flux partitioning was based on Reichstein et al. (2005). All FLUXNET information and downloading instructions are at https://daac.ornl.gov/cgi-bin/dataset_lister.pl?p=9 (accessed on 26 March 2021)

3. Global monthly average GPP (g carbon m^{-2} d^{-1}) modeled at 8 km spatial resolution for each of the 35 yr from 1982 to 2016. GPP is based on the well-known Monteith LUE. LUE was extrapolated to a consistent 8 km resolution global grid using multiple explanatory variables representing climate, landscape, and vegetation factors influencing LUE and GPP. Global gridded long-term daily GPP was derived using the canopy fraction of photosynthetically active radiation from the Global Inventory Modeling and Mapping Studies (GIMMS3g), and meteorological information from Modern-Era Retrospective analysis for Research and Applications, Version 2, (MERRA-2; Madani & Parazoo, 2020), available at https://daac.ornl.gov/cgi-bin/dsviewer.pl?ds_id=1789, accessed on 25 March 2021

4. Global Land Evaporation Amsterdam Model 1, 2 (GLEAM) is a set of algorithms that estimate the different components of land evaporation (i.e., evapotranspiration) separately based on satellite observations: transpiration, interception loss, and other evaporation terms. This characteristic allowed us to observe the interception of rainfall by the forest canopy separate from subsequent evaporation into the atmosphere, which constitutes an important part of the hydrological balance in forest regions (Cuartas et al., 2007; Czikowsky & Fitzjarrald, 2009; Miralles et al., 2010). GLEAM v3.5a is a global data set spanning the 41 yr period from 1980 (1 January) to 2020 (31 December). It is available at https://www.gleam.eu/ and was accessed on 24 March 2021, for this study. The data set is based on satellite and reanalysis data (ERA5 net radiation and air temperature; Martens et al., 2016, 2017; Miralles, de Jeu, Gash, Holmes, & Dolman, 2011; Miralles et al., 2010; Miralles, Holmes, et al., 2011)

5. TerraClimate is a high-spatial-resolution data set (1/24°, ~4 km) of monthly climate and water balance for global land surfaces in the period 1958–2015. TerraClimate interpolates high-spatial-resolution climatological data from the WorldClim data set to produce a monthly data set of precipitation, temperature, wind speed, vapor pressure, and solar radiation. It can be accessed at http://www.climatologylab.org/terraclimate.html. TerraClimate produces monthly surface water balance data sets using a water balance model that incorporates evapotranspiration, precipitation, and temperature as reference. The spatio-temporal aspects of TerraClimate are validated using annual temperature, precipitation, and reference evapotranspiration calculated from station data, as well as observed annual runoff from streamflow gauges (Abatzoglou et al., 2018)

2.3. Analysis of the Influence of LUC and Atmospheric CO_2 on GPP

We used the following equation to infer the influence of land use changes and eCO_2 on a variable (VAR) that can be GPP or evaporation:

$$VAR = VAR_{LUC\,hist\,CO_2} - VAR_{PNV\,const\,CO_2} \tag{1}$$

To see the influence of LUC on evaporation and GPP, we used the following equation:

$$VAR = VAR_{LUC\,hist\,CO_2} - VAR_{PNV\,hist\,CO_2} \tag{2}$$

Finally, Equation 3 was used to analyze the exclusive effect of CO_2 fertilization under LUC:

$$VAR = VAR_{LUC\,hist\,CO_2} - VAR_{LUC\,const\,CO_2} \tag{3}$$

WUE, which is the amount of carbon gained per unit of water loss at the ecosystem level is calculated as follows:

$$WUE = GPP/Tr \tag{4}$$

Where Tr is vegetation transpiration. WUE (kg m^{-2} mm^{-1} month^{-1}) was calculated for all the conditions of CO_2, LUC, and PNV defined in the scheme of Figure 2.

2.4. Analysis of Probable Climate Changes

In order to verify climate changes that could have occurred in the southern Amazon in the period 1981–2010, we analyzed precipitation, air temperature, shortwave downward radiation, and specific humidity values in GLDAS, GSWP3, and WATCH + WFDEI that were used as input to the DGVMs. Ensemble means were estimated with these data and then divided into two periods: 1981–1995 (P1) and 1996–2010 (P2). Seasonal averages (dry and rainy seasons) were calculated for each period. To visualize differences we subtracted P1 from P2.

3. Results

3.1. Statistical Distribution of GPP, Evaporation (E), Transpiration, Interception, and WUE

In this section, we show the distribution of data in DGVM simulations for GPP, evaporation, transpiration, interception, and WUE in the dry and rainy seasons, under the LUC hist CO_2 condition. These results are compared with data sets of "observed data" (Section 2.2.3).

The highest GPP in the dry season (JJAS) was estimated through the LUE and had its median above 0.25 kg m^{-2} month^{-1} (Figure 3a). With the eddy covariance method, GPP distribution showed a low error and concentrated around 0.21 kg m^{-2} month^{-1}. Similarly, the GPP estimated by FLUXCOM (RS + meteo + ANN) also had concentrated distribution and little variation; however, it was lower in the dry season, around 0.1.5 kg m^{-2} month^{-1} (Figure 3a). As to modeled GPP, INLAND, and ORCHIDEE had higher GPP values than LPJ-GUESS and LPJmL4, with medians ranging between ~0.21 and ~0.15 kg m^{-2} month^{-1}, depending on the climatic forcings GLDAS, GSWP3, and WATCH + WFDEI. The variation range in LPJ GUESS and LPJmL4 was 0.05 and 0.1 kg m^{-2} month^{-1} respectively in the dry season (Figure 3a). In the rainy season (JFMA), the LUE-estimated GPP was close to 0.28 kg m^{-2} month^{-1}, which is the highest value of GPP estimates, higher than all the DGVMs and other observed data. INLAND and ORCHIDEE also had high GPP values, with medians ranging between 0.25 and 0.29 kg m^{-2} month^{-1} respectively. In LPJ-GUESS LPJmL4, the medians ranged from 0.15 to 0.19 kg m^{-2} month^{-1} for climatic forcings (Figure 3b).

Evaporation values from FLUXCOM (RS + meteo + ANN) and GLEAM were close to the medians (~93 and ~96 mm month^{-1}) for the dry season, while TerraClimate was close to 75 mm month^{-1}. Among the DGVMs, INLAND had the highest values (~110 and ~116 mm month^{-1}) of all DGVMs. In the other models (LPJ-GUESS, LPJmL4, and ORCHIDEE), medians were between ~40 and ~65 mm month^{-1}; except for GLDAS-forced LPJ-GUESS (in blue) which reached ~100 mm month^{-1} (Figure 3c). The high evaporation values from INLAND in the dry season might be explained by INLAND's sensitivity to radiation. In the rainy season, FLUXCOM (RS + meteo + ANN) and GLEAM had near-median values (121–125 mm month^{-1}), while TerraClimate was close to 85 mm month^{-1}. Of all the DGVMs, LPJ-GUESS reached the highest median values ranging from ~100 to ~120 mm month^{-1} (Figure 3d).

Regarding transpiration, GLEAM estimated high median values (~80 mm month^{-1}) for the dry season compared to the other DGVMs whose results were between ~40 and 59 mm month^{-1}, except for INLAND, which had values between 90 and 98 mm month^{-1} (Figure 3e). For the rainy season, GLEAM estimated transpiration at around 84 mm month^{-1}, contrary to INLAND which showed very low values ~39 and 42 mm month^{-1} (Figure 3f).

The median interception was estimated at less than 20 mm month^{-1} in the dry season, with the exceptions of LPJ-GUESS with GLDAS forcing and INLAND with WATCH + WFDEI forcing (Figure 3g). In the rainy season, INLAND simulations reached very high interception, between ~58 and 74 mm month^{-1}; GLEAM, 40 mm month^{-1}; while in the other DGVMs, the median interception was below 40 mm month^{-1} (Figure 3h). We are aware that INLAND overestimates the leaf area index (LAI), which justifies the high interception values we present in Figure 3h.
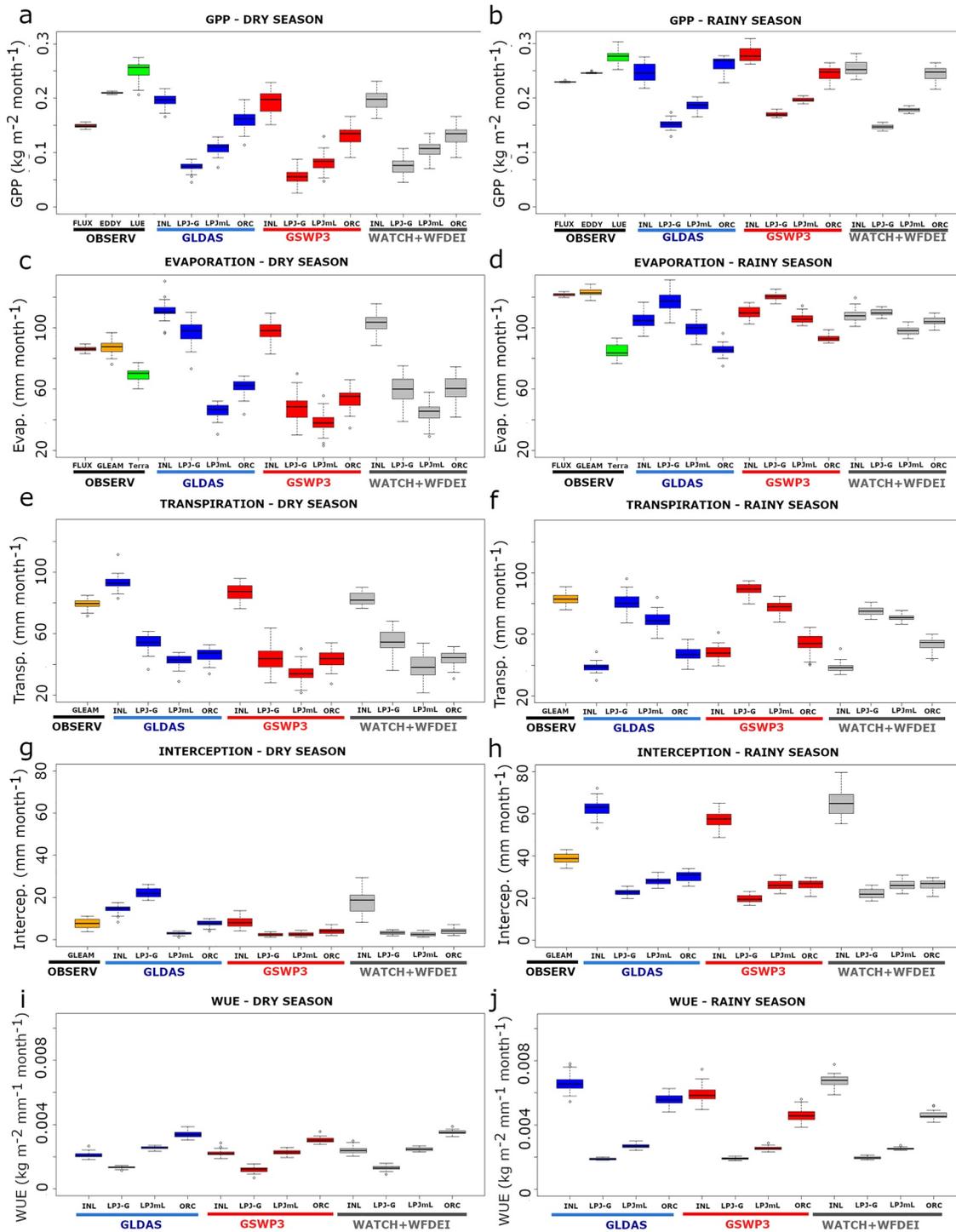
Figure 3. Statistical distribution of GPP, evaporation, transpiration, interception, and WUE for LUC historical CO_2, observables (OBSERV) (FLUX: FLUXCOM, EDDY: network of eddy covariance towers, LUE: Light Use Efficiency, GLEAM, and Terra: TerraClimate) and DGVM outputs with forcings GLDAS (blue), GSWP3 (red), and WATCH + WFDEI (gray), for the dry season (JJAS) on the left and the rainy season (JFMA) on the right panels.

WUE was higher in ORCHIDEE than in the other models in both seasons. Since WUE = GPP/Transpiration is related to precipitation, INLAND also estimated high values for WUE in the rainy season. In fact, INLAND-simulated WUE was the highest of all DGVMs, because it had both high GPP and the lowest transpiration (Figures 3i and 3j).
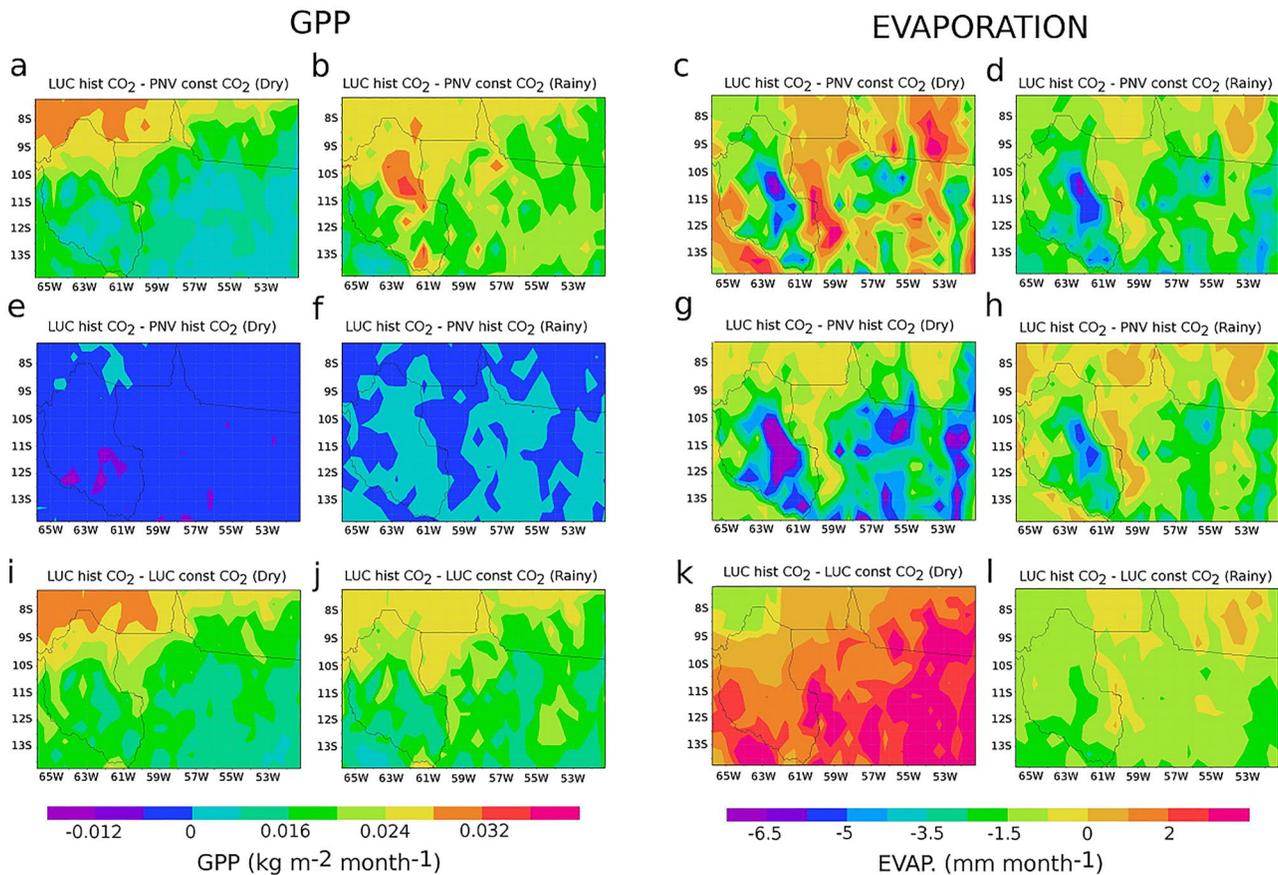
Figure 4. Ensemble of DGVM results for GPP and evaporation in the dry (JJAS) and rainy (JFMA) seasons—application of equations of Section 2.3 to identify LUC and eCO2 joint and individual effects.

3.2. Results From Applying Section 2.3 Equations on the DGVM Ensemble

3.2.1. GPP

The result of applying equation LUC hist CO_2 minus PNV const CO_2 (a) on the ensemble of DGVMs to infer the influence of land use changes and eCO_2 revealed a clear increase in GPP (positive values) over the entire study region (Figures 4a and 4b), with the highest values in the rainy season (Figure 4b). As a result of equation LUC hist CO2 minus PNV hist CO2 (b) (LUC effect), a very slight increase was observed in GPP, whose values were close to zero in general, and even below zero in the dry season (Lon: 61°–64°W, Lat: 11°–13°S). In the rainy season, precipitation seems to have contributed to a slight increase in GPP (Figures 4e and 4f). When applying equation LUC hist CO_2 minus LUC const CO_2 (c) for the eCO_2 effect, we obtained positive GPP values over the entire study area in both seasons (Figures 4i and 4j).

3.2.2. Evaporation

The joint effect of LUC and eCO_2 (Equation 1) in the dry season, resulted in a positive balance of up to 2 mm month^{-1}, however, deficits were greater, up to 6 mm month^{-1} (Figure 4c). In the rainy season, evaporation deficit was observed over almost the entire study region (Figure 4d). Equation 2, LUC hist CO_2 minus PNV hist CO_2 showed that evaporation in the dry season was more negative and expanded over a larger area than in the other simulations (Figure 4g). In the rainy season, evaporation was also negative over the entire study region, although it was less intense than in the dry season (Figures 4g and 4h). For the eCO_2 effect, applying the equation LUC hist CO_2 minus LUC const CO_2 (Equation 3), the balance was positive over almost the entire region in the dry season. Contrarily, in the rainy season, the balance was negative over almost the entire region and did not exceed 1.5 mm month^{-1}.

Table 1
Variation of GPP (kg m^{-2} month^{-1}) and Evaporation (mm month^{-1}) in the Dry (JJAS) and Rainy (JFMA) Seasons Under Different LUC and CO$_2$ Concentration Conditions

	LUC hist CO$_2$ (mean)	LUC const CO$_2$ (mean)	PNV hist CO$_2$ (mean)	PNV const CO$_2$ (mean)	LUC hist CO$_2$-PNV const CO$_2$	LUC hist CO$_2$-PNV const CO$_2$ (%)	LUC hist CO$_2$-LUC const CO$_2$	LUC hist CO$_2$-LUC const CO$_2$ (%)	LUC hist CO$_2$-PNV hist CO$_2$	LUC hist CO$_2$-PNV hist CO$_2$ (%)
GPP (dry)	0.1269	0.1073	0.1310	0.1098	0.0171	13.47	0.0196	15.4	−0.0041	−3.23
GPP (rainy)	0.2123	0.1926	0.2117	0.1901	0.0222	9.27	0.0197	9.27	−0.0004	−0.18
Evap. (dry)	65.07	63.36	67.66	65.59	−0.52	−0.79	1.71	2.62	2.59	−3.98
Evap (rainy)	99.91	100.87	101.14	101.74	−1.83	−1.83	−0.96	−0.96	−1.23	−1.23

The comparison of LUC hist CO$_2$ with LUC const CO$_2$ revealed that the effect of CO$_2$ fertilizer was determinant for GPP. Mean values were 0.1269 kg m^{-2} month^{-1} for LUC hist CO$_2$ and 0.1073 kg m^{-2} month^{-1} for LUC const CO$_2$ in the dry season. The means differed by 15.4% (0.0196 kg m^{-2} month^{-1}; Table 1). In the rainy season, the mean value of LUC hist CO$_2$ was ∼0.2123 kg m^{-2} month^{-1} and ∼0.1926 kg m^{-2} month^{-1} for LUC const CO$_2$, with a difference of 0.0197 kg m^{-2} month^{-1}, which corresponds to 9.27% (Table 1).

The effects of LUC on evaporation had some significance in the comparison of LUC hist CO$_2$ with PNV hist CO$_2$, with evaporation decreasing by about 3.8% (Table 1). Average values over the region were attenuated due to the dense forest cover in the sub-regions located in the northwest, where evaporation remained the same. Comparing Figure 4g with the data in Table 1, we can see that for the LUC effect (LUC hist CO$_2$ minus PNV hist CO$_2$) the regions with the greatest evaporation deficit (−6.5 mm month^{-1}; 61°–63°W, 10°–13°S; 51°–52° W, 10°–14°S) were the ones with the most intense deforestation. The deficit represents a decrease of 9.98% in evaporation in the dry season. The effects of condition LUC hist CO2 minus PNV hist CO$_2$ on evaporation had some significance when the decrease was about 3.98% (Table 1) in the dry season.

When we look at the distribution of DGVM ensemble data, GPP and evaporation present greater dispersion in the dry season than in the rainy season (Figure 5). Under conditions PNV hist CO$_2$ and PNV const CO$_2$, there was no significant decrease in mean GPP, contrary to what was noted for LUC const CO$_2$. The greater forest cover compensates for the absence of the CO$_2$ fertilization effect as in PNV const CO$_2$ in which the distribution of data is slightly higher than in LUC hist CO$_2$ (Figure 5a). Evaporation was also slightly higher in PNV (hist CO$_2$ and const CO$_2$), mainly in the dry season than in both seasons under LUC (hist CO$_2$ and const CO$_2$; Figure 5b).

3.3. DGVM Forcings and Results

For the analysis of precipitation, Figure 6 shows the standard deviation (std) of the seasonal (dry and rainy season) ensemble (Figures 6a and 6b), the seasonal ensemble mean (Figures 6c and 6d); and the seasonal mean for each data set (GLDAS, GSWP3, and WATCH + WFDEI) in Figures 6e–6j). A precipitation pattern can be observed in GSWP3 and WATCH + WFDEI. The standard deviation of the DGVM ensemble in the dry season was around 15 mm month^{-1} and occurred sparsely in some sub-regions (Figure 6a). In the rainy season, the standard deviation of the DGVM ensemble reached higher values, around 30 mm month^{-1} in the west of our study region (Figure 6b). The greatest uncertainties (highest std) in both seasons were around 53°–55°W and 7°–9°S; 63°–65°W and 9°–12°S (Figures 6a and 6b). The highest rainfall averages (up to ∼350 mm month^{-1}) were observed in the north of our study region between 52°–64°W and 7.5°–9.5°S, mainly for GSWP3 and WATCH + WFDEI. On the other hand, the region with the lowest average rainfall (∼20 mm month^{-1}) was between 53°–57°W and 11°–14°S; 62°–64°W and 12°–14°S. The region with the highest average rainfall suffered less deforestation than the southern part of our study region, where the anthropogenic impact was most intense (D. S. Alves, 2002; Cardille & Foley, 2003). Moreover, for precipitation, we observed that there was a greater agreement for GSWP3 and WATCH + WFDEI in both seasons (Figure 6). However, GLDAS strongly disagrees with these two data sets. Ahlström et al. (2017) argue that the greatest uncertainties of Earth system models to estimate future climate and vegetation for the Amazon are in the precipitation forcing data.

We analyzed the influence of precipitation (P) and shortwave radiation (SW) on simulated GPP and evaporation. INLAND and ORCHIDEE showed high P x GPP correlation in a range of 0.71–0.82 in the dry season
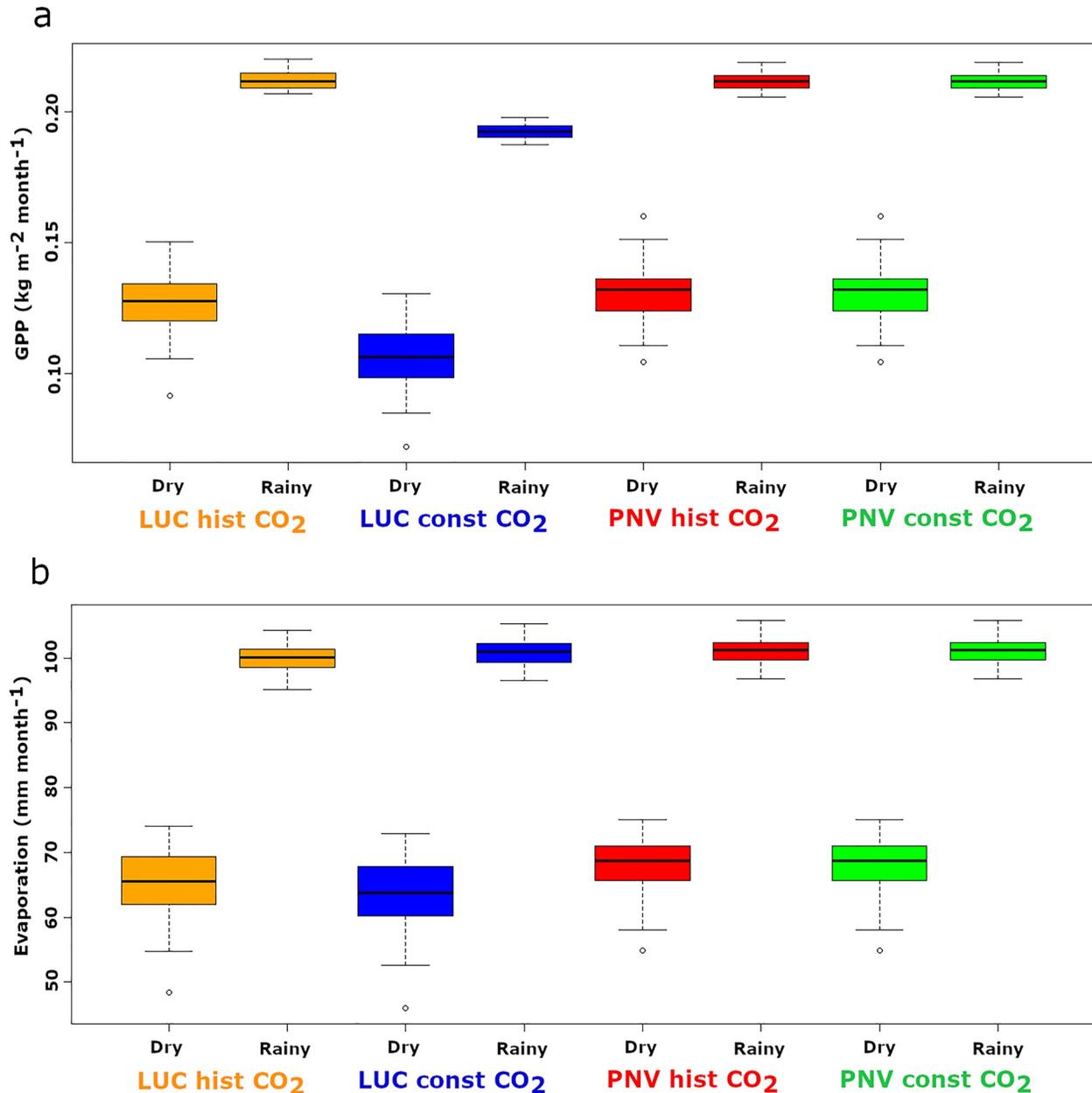
Figure 5. Distribution of gross primary productivity (GPP) and evaporation data in the dynamic global vegetation models (DGVM) ensemble in the dry (JJAS) and rainy (JFMA) seasons.

(Figures 7a, 7e, 7i and 7d, 7h, 7l, respectively); in LPJ-GUESS and LPJmL4 correlation was negative with values reaching −0.56 and there was no correlation in other cases (Figures 7b, 7f, 7j and 7c, 7g, 7k, respectively).

In the rainy season, INLAND showed a moderate negative P X GPP correlation of between −0.31 and −053; LPJ-GUESS showed weaker (0.20) or no correlation and most of the sample was between 0.15 and 0.25 kg m^{-2} $month^{-1}$. In another part of the sample (fewer cases), GPP values were close to 0.1 kg m^{-2} $month^{-1}$ and can be considered as outliers or spurious data; LPJmL4 had a moderate correlation (from 0.39 to 0.67) as well as ORCHIDEE with values between 0.37 and 0.43 (Figures S10b, S10f, S10j—Supporting Information).

In the dispersion plots, shortwave (SW) was between ∼185 and 240 W m^{-2} day^{-1} and evaporation ranged from 30 to 140 mm $month^{-1}$ in the dry season (Figure S11—Supporting Information). A negative SW x E correlation between −0.22 and −0.75 predominated, with only one case of positive correlation of 0.29 in INLAND with the
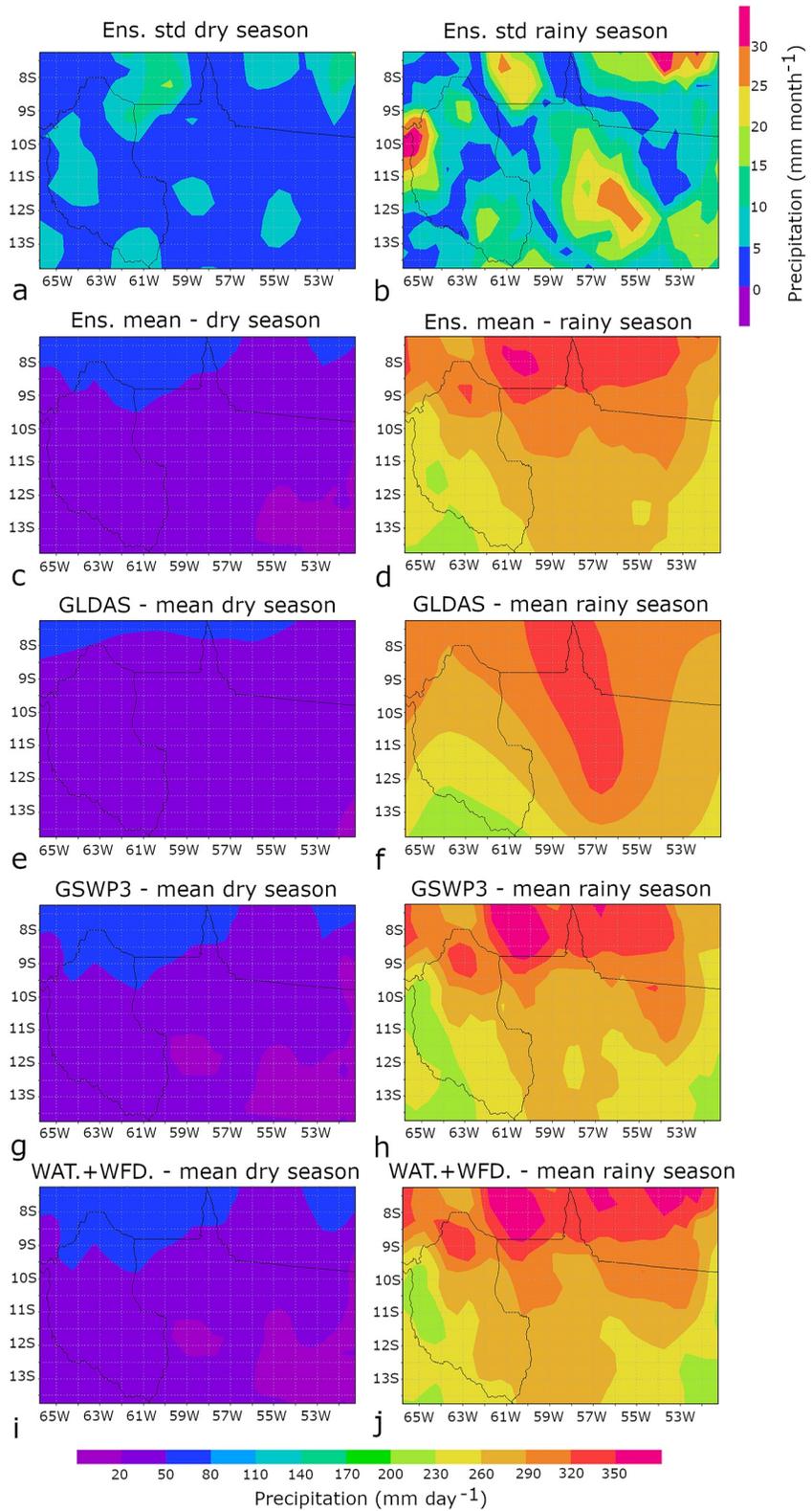
Figure 6. Seasonal ensemble of precipitation in the dry (JJAS) and rainy (JFMA) seasons: standard deviation (a, b); seasonal ensemble means (c, d); and seasonal means of data sets GLDAS, GSWP3, and WATCH + WFDEI (e–j).
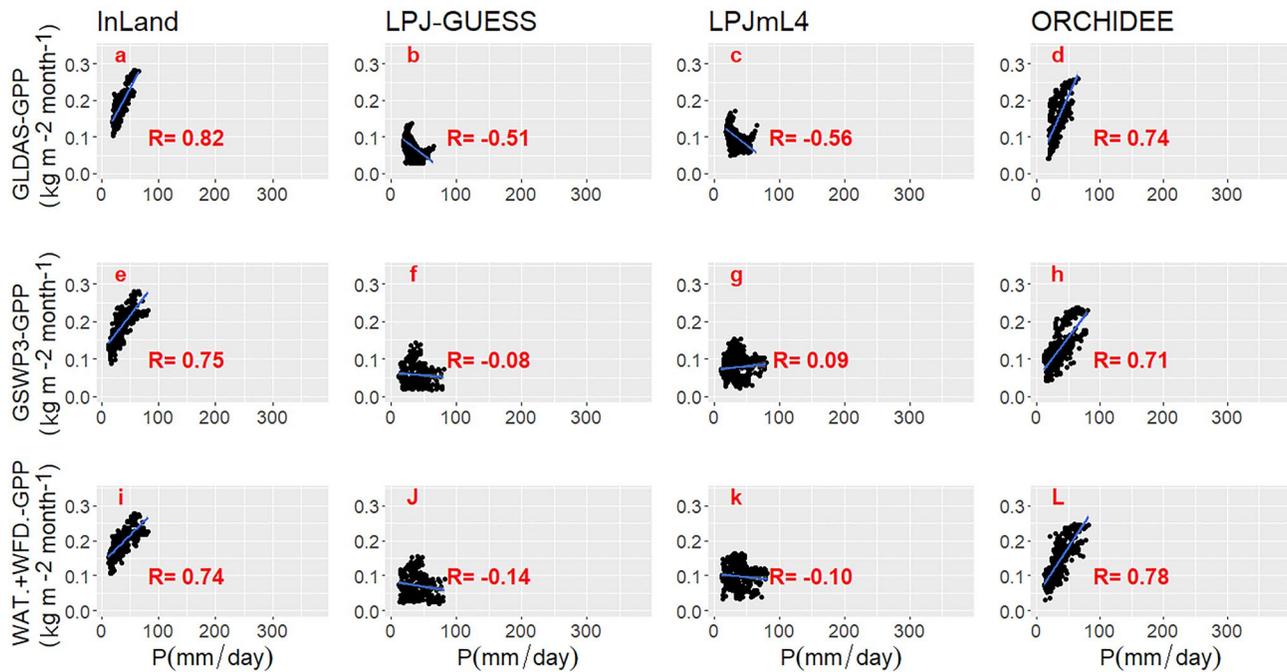
Figure 7. Dry season (JJAS): Precipitation (P) x GPP—all DGVMS and data sets.

GLDAS data set (Figure 8a). Only LPJmL4 with WATCH + WFDEI presented no correlation (Figure S11—Supporting Information).

SW was between 50 and 215 W m^{-2} day^{-1} and E varied between 80 and 130 mm day^{-1} in the rainy season. Still, for the rainy season, most cases of SW x E correlation were negative between −0.22 and −0.64. INLAND was the exception, as it had a positive SW x E correlation between 0.12 and 0.45. No correlation was seen in the remaining cases. (Figure S12—Supporting Information).

3.4. Analysis of Climate Forcings in the Region

We analyzed the forcings used as input in the simulations to look for some evidence of regional climate change. We observed an increase in air temperature over almost the entire study region in the dry season. The warming was as much as 1°C (51°–53°W, 7.5°–11.5°S; Figure 8a). In the rainy season, the temperature rise was also observed in almost the entire region, but it did not exceed 0.6°C (Figure 8b). We only observed a slight decrease in air temperature (0.1°C) over the Bolivian part of the study region (65°–66°W, 12.5°–13.5°S).

For the shortwave variable, we observed an increase up to 5.5 W m^{-2} month^{-1} in the dry season in the entire study region (52°–53°W, 8°–9°S; Figure 8c). The regions of increased SW are partially coincident or close to those where warmer temperatures were observed in the dry season. In the rainy season, the observed increase was up to 4 W m^{-2} month^{-1}. We also observed a decrease to 3 W m^{-2} month^{-1} over Bolivia.

As for specific humidity, the greatest decrease occurred in the dry season reaching 0.003 (multiplied by 1,000; 51°–53°W, 7.5°–10.5°S). In the region of Bolivia (63°–66° W, 11°–14°S) there was an increase in humidity of around 0.0005. In the rainy season, specific humidity rose throughout the study region.

Precipitation decreased to 15 mm month^{-1} in almost the entire region (56°–58°W, 10.5°–12.5°S) during the dry season. In the rainy season, the drop reached 30 mm month^{-1} (55°–57°W, 9°–13°S). We also observed an increase in precipitation, up to 20 mm month^{-1}, over Bolivia (65°–66°W, 12°–13°S).

The analysis of the distribution of mean air temperature and precipitation in the dry and rainy seasons in each of the periods P1 (1981–1995) and P2 (1996–2010) revealed an increase in temperature in both seasons of P2 (Figure 9). Precipitation showed a decline in both seasons of P2. The variation in the rainy season was greater in P2 than in P1.
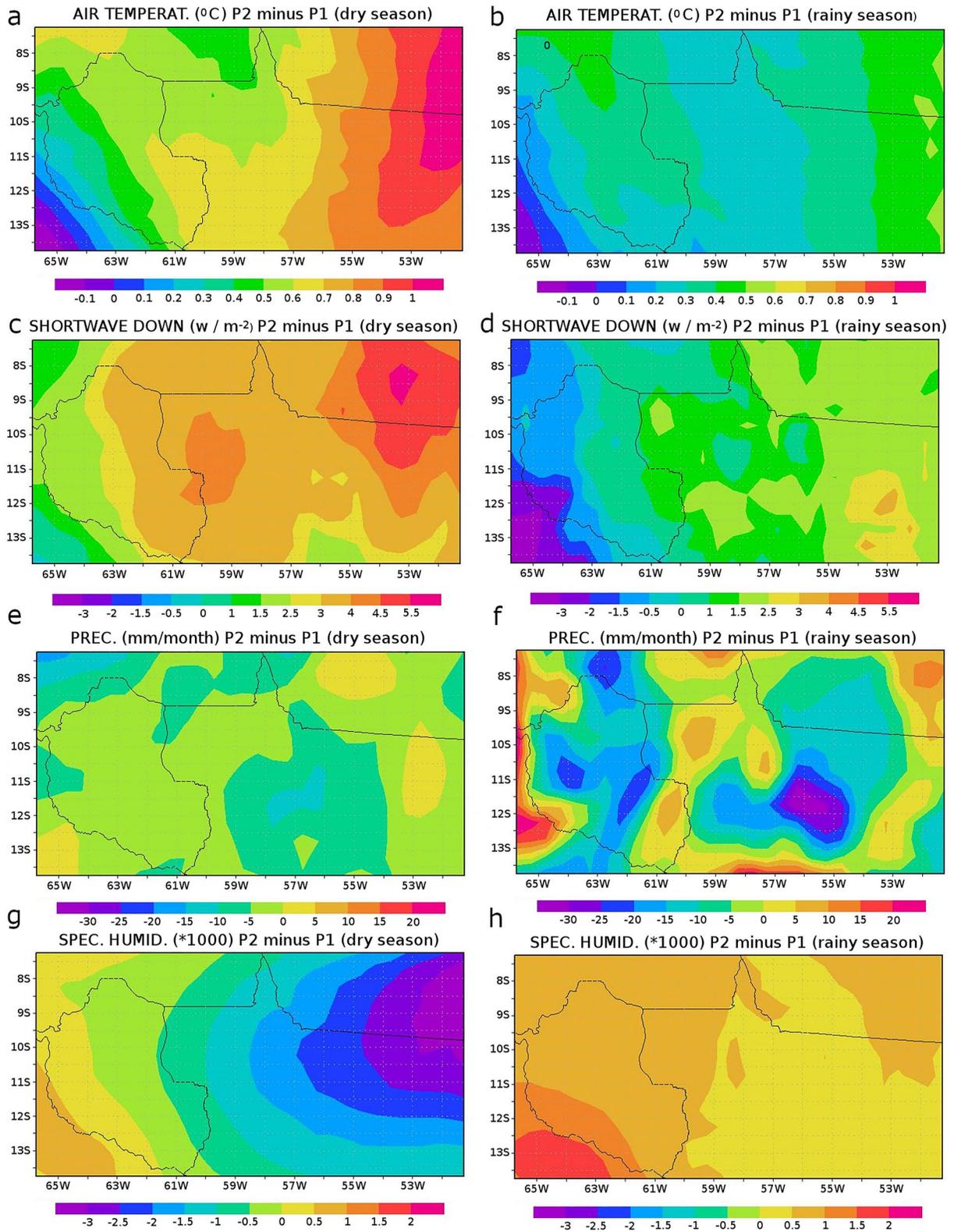
Figure 8. Climate forcings—difference between Period 2 (P2) (1996–2010) and Period 1 (P1) (1981–1995).
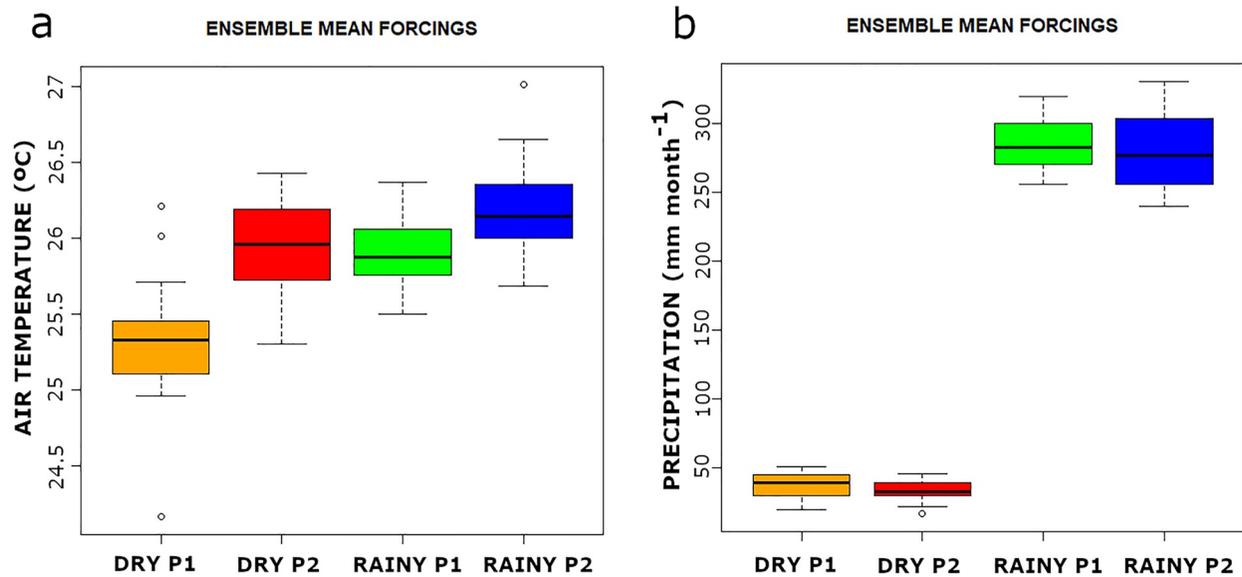
Figure 9. Data distribution for the ensemble mean of air temperature and precipitation (forcings)—dry (JJAS) and rainy (JFMA) seasons—Period 1 (P1) (1981–1995) and Period 2 (P2) (1996–2010).

4. Discussion

4.1. Gross Primary Productivity (GPP)

FLUXCOM data estimate GPP based on the fraction of absorbed photosynthetically active radiation (fAPAR). It applies LUE functions and LAI satellite measurements (Baldocchi et al., 2001; Jung et al., 2020). These FLUX-COM data were useful as a reference for an approach other than that of DGVMs. FLUXCOM data involve remote sensor monitoring and flux tower measurements, so we consider them "observed data".

We recognize that FLUXCOM data have uncertainties that are tied to the methodology, such as the thickness of clouds, which makes remote sensing measurements difficult in tropical regions (Ryu et al., 2019; Valentini et al., 2014), low density of flux towers to cover large areas (Ometto, Aguiar, Assis et al., 2014; Schimel et al., 2015), and errors inherent to the eddy covariance estimation process (Restrepo-Coupea et al., 2013; C. Von Randow et al., 2008; Yi et al., 2010). However, we used these FLUXCOM data as a reference to compare the influence of LUC on GPP DGVM simulations.

The results showed that LPJ-GUESS and LPJmL4 had GPP values significantly lower than INLAND and ORCHIDEE. The disagreement among DGVMs and Earth System Models (ESMs) concerning vegetation was discussed by Ahlström et al. (2017), who attribute a large part of the differences to the way models deal with mortality and disturbance. INLAND and ORCHIDEE do not explicitly simulate detailed tree mortality but instead, they use a defined carbon residence time. In INLAND, the residence time has a temporal resolution of years for native vegetation and days for crops (Kucharik et al., 2000). In ORCHIDEE, the residence time is considered only for the removal of woody PFTs, while mortality of plantations and pastures is driven by seasonality (and leaf longevity) and deciduous PFTs. Only one supplementary term corresponds to seasonal mortality (i.e., leaves and fine roots) which is based on two terms: one related to leaf longevity (i.e., when leaves reach longevity, the turnover increases rapidly); the other one is related to climate (Krinner et al., 2005). In the process of phenology, it is a trigger for trees: when temperature or soil water in tropical regions falls below a threshold, senescence is triggered and leaves fall within a predefined period (Krinner et al., 2005). Tree mortality in LPJ-GUESS can result from stress, background factors such as senescence and small-scale disturbance, and large-scale disturbances. Mortality results in a reduced population or cohort density and the biomass of dead individuals is transferred to the litter pool, except in the case of fire mortality, where the affected biomass is lost in the form of a CO_2 flux to the atmosphere (B. Smith, 2001). In LPJmL4, tree mortality results from low productivity, background mortality, and post-fire mortality (Schaphoff et al., 2018). As

can be seen, the DGVMs used in this experiment deal with fire differently. While the other DGVMs have their own modules, INLAND uses the sub-module of the Canadian Terrestrial Ecosystem Model (CTEM; Arora & Boer, 2005). However, DGVMs consider some aspects for fire ignition to occur, such as low soil moisture/litter, and high temperatures and low precipitation, among others (Schaphoff et al., 2018). The burned area is assumed nonlinearly and the vegetation that will burn depends on the specific resistance parameter of PFT for woody plants, while all litter and living grasses are consumed by fire. Yet, fire spreading also depends on litter moisture. This is the usual way fire is implemented in DGVMs and how it contributes to changes in land cover (Schaphoff et al., 2018).

However, the major issue with GPP concentrates around photosynthesis, that is, the process of carbon assimilation by vegetation. All the models used in this work (INLAND, LPJ-GUESS, LPJmL4, and ORCHIDEE) basically adopt the photosynthesis model proposed by Farquhar, von Caemmerer, and Berry (FvCB; Farquhar et al., 1980), with some differences and additions. For example, in addition to what was proposed by Farquhar et al. (1980), photosynthesis parameters in LPJ-GUESS, LPJmL4, and ORCHIDEE are based on Collatz et al. (1991, 1992). There are also differences in stomatal conductance among models. INLAND, which is derived from the IBIS model (Foley et al., 1996), is based on Collatz et al. (1991, 1992), and Leuning (1995); LPJ-GUESS and LPJmL4 are based on Haxeltine and Prentice (1996); and ORCHIDEE is based on Ball et al. (1987). Although these approaches do not differ much from each other, small differences in the implementation can contribute to larger differences among model results. In addition, several other physiological variables are not similarly parameterized.

Although we have not analyzed the values inferred by the DGVMs in this work, we know that the calculation of the maximum carboxylation velocity (Vc_{max}), that is, the process velocity by which Rubisco (the most abundant enzyme in plants) catalyzes ribulose-1,5 biphosphate (RuBP) molecules with CO_2 to produce the carbon compounds, has different ways of approach and treatment in the models (Rogers, 2014). The values of Vc_{max} used in the models vary markedly with identical Plant Functional Types (PFTs; Rogers, 2014). Thus, several uncertainties have been observed in DGVM simulations which tend to underestimate maximum GPP (Bonan et al., 2012; Dietze, 2014). This variation among models can be attributed to the lack of data used for proper Vc_{max} calibration and to the use of canopy level Vc_{max} values, which are lower than those observed at the leaf level (Dietze, 2014; Rezende et al., 2015). For this reason, it is important that Vc_{max} be well-calibrated or that the estimation of this parameter be as realistic as possible because it has a direct impact on GPP models (Bonan et al., 2012; De Kauwe et al., 2015; Dietze, 2014; LeBauer et al., 2013; Rogers, 2014; N. G. Smith & Dukes, 2012).

Another important physiological issue is the limitation of nutrients (nitrogen and phosphorus) needed in the carbon acquisition process, which consequently affects GPP. In our experiment, only INLAND does not deal with nitrogen in this photosynthetic process (Rezende et al., 2015). The other DGVMs: LPJ-GUESS, LPJmL4, and ORCHIDEE assume photosynthetic capacity as conditioned by leaf nitrogen content (Hickler, 2012; Krinner et al., 2005; Schaphoff et al., 2018; Sitch et al., 2003). This may partly explain the significantly higher GPP values of INLAND compared to the other DGVMs.

However, regarding the experiment we conducted specifically, the decisive factor in the calculation of GPP was the LAI estimated in the DGVMs. In the case of INLAND, the LAI is overestimated (1–11 $m^2\,m^{-2}$; Table 2), even though in our study region with tropical evergreen vegetation, LAI values in INLAND are always the highest, in the range of 8–11 $m^2\,m^{-2}$ (Kucharik et al., 2000). The reason of INLAND is calculating higher LAI values, it may be that they are also overestimating the carbon allocation in the leaves which is a variable that will influence in this calculation (Equation S3 in Supporting Information S1). The calculation of LAI can also be influenced by the variable specific leaf area that in INLAND is parameterized for each PFT as shown in the Equation S3 in Supporting Information S1. A high LAI will lead to high GPP rates and we demonstrate this dependency for INLAND (Equation S4 and Figure S2 in Supporting Information S1) and for ORCHIDEE (Figure S3 in Supporting Information S1). In both DGVMs, the correlation was 0.73. LAI values in LPJ-GUESS and LPJmL4 are lower (1–6 $m^2\,m^{-2}$). Consequently, LPJ-GUESS and LPJmL4 had lower GPP values compared to INLAND, ORCHIDEE as well as to the FLUXCOM, eddy covariance and LUE approaches, mainly in the rainy season (Figure 3). Thus, we can see that DGVMs whose highest LAI values are around 10–11 $m^2\,m^{-2}$, had higher GPP rates like INLAND. On the other hand, for those with the highest LAI values around 6 $m^2\,m^{-2}$, such as LPJ-GUESS and LPJmL, the estimated GPP was around 50% lower than INLAND and ORCHIDEE.

Table 2
Range of DGVM-Estimated Leaf Area Index (LAI; Maximum Value for Tropical Evergreen Vegetation; Krinner et al., 2005; Kucharik et al., 2000; Schaphoff et al., 2018)

	INLAND	LPJ-GUESS	LPJmL4	ORCHIDEE
LAI (range)	1–11($m^2 m^{-2}$)	1–6 ($m^2 m^{-2}$)	1–6 ($m^2 m^{-2}$)	1–10 ($m^2 m^{-2}$)

Plant growth is modeled by the variation of the LAI and biomass of each PFT. A grid cell can contain one or more types of functional plants (PFT), which together form a type of vegetation. All PFTs can grow anywhere within their bioclimatic limits, that is, the model considers that changes in the composition and structure of vegetation occur in response to environmental conditions. This explains the compensation in GPP: when switching from PNV constant CO_2 to LUC historical CO_2, the part of native vegetation that is deforested within a grid cell is occupied by grasses that continue to sequester carbon at higher rates of fertilization.

In addition to physiological issues, divergence in results can be generated by the fact that models use different processing strategies, sometimes even to avoid numerical errors and anomalous situations. For example, when INLAND calculates intercellular CO_2 concentration, it weighs the results obtained at previous stages by iteration to prevent the occurrence of anomalous values. Intercellular concentration has a direct effect on increasing GPP. The models discussed here demonstrated this sensitivity to CO_2 (Figure 4 and Table 1)

4.2. Evaporation (E)

The results for the dry season (Figure 4g) showed that LUC was decisive in reducing evaporation in the balance LUC hist CO_2 minus PNV hist CO_2. C. Von Randow et al. (2004) observed that in regions of intense LUC (conversion of forests to pastures), the evaporative rate in the dry season could be 20%–41% lower than in forests. Even in the rainy season, evaporation on pastures can be 17% lower than in the forest. Another reason may be the increase in net radiation, often observed in the Amazon during the dry season (Harper et al., 2014). INLAND has also been observed to be very sensitive to radiation and we can see in Figure S2 in Supporting Information S1 (a, e, i) that evaporation for INLAND reached values close to 150 mm month^{-1} in the dry season, while in the other DGVMs it was below 100 mm month^{-1}. Still, in the dry season, we can see that shortwave that had an effect on evaporation was in the range of ~175 to ~240 (w m^{-2} day^{-1}) for all DGVMs having GLDAS and GSWP3 forcings (Figures S2a–S2h in Supporting Information S1). On the other hand, for the WATCH + WFDEI forcing, shortwave in all DGVMs had intermediate values ~185–115 (w m^{-2} day^{-1}; Figures S2i– S2l in Supporting Information S1). The reason for the high values observed in INLAND with respect to the other DGVMs in the dry season (Figures S4a, S4e, S4i in Supporting Information S1) is that higher LAI along with higher stem area index (SAI) cause greater absorption of radiation which contributes to the evaporation from the wet surfaces of these leaves and stems (Equation S5 in Supporting Information S1). In addition, higher LAI means higher transpiration rates and higher rainfall interception, with consequent greater water availability (Figure 3). In the rainy season, all DGVMs have similar patterns for GLDAS and GSWP3 forcings, and shortwave was between 170 and 215 w m^{-2} day^{-1}; on the other hand, for the WATCH + WFDEI forcing, shortwave was between 150 and 200 w m^{-2} day^{-1}.

These results showed large differences among models. Sörensson and Ruscica (2018) argue that the mechanisms driving evaporation, mainly during the dry season and in more seasonal climates such as that of southern Amazonia, are still poorly understood, which would explain the differences in model results. While evaporation seems to be overestimated by INLAND compared to FLUXCOM and GLEAM, it seems to be underestimated by LPJ-GUESS and LPJmL4. One probable explanation for this underestimation may lay in plant rooting strategies, because they have developed a wide variety of rooting strategies to have access to water, and DGVMs often condense this variety of rooting strategies into averages on a biome scale (Sakschewski et al., 2020). This type of biome-scale averaging procedure has led to unrealistic evaporation values. Sakschewski et al. (2020) used the DGVM LPJmL4.0-VR (derived from LPJmL4) in which simulations begin with an even distribution of tree rooting strategies for each PFT (tropical and deciduous evergreen) at each location, and this distribution is driven by environmental and competition conditions. In simulations on the Amazon, Sakschewski et al. (2020) reported that they obtained more realistic evaporation values. Their results showed values close to

Table 3
Summary of Questions on GPP, Evaporation, and WUE Results

Issue	Explanation
Differences in GPP among DGVMs	INLAND does not deal with nutrient (nitrogen) limitation (Rezende et al., 2015). Differences in the parameterization and in the processes of inferring physiological variables (Bonan et al., 2012; De Kauwe et al., 2015; Dietze, 2014; LeBauer et al., 2013; Rogers, 2014; Smith & Dukes, 2012). LAI overestimated in INLAND will run into high GPP rates (Figure S2 and Equation S4in Supporting Information S1). High LAI values may result in overestimation of the carbon allocation calculation in the leaves and the parameterization of the specific leaf area (Equation S3in Supporting Information S1). On the other hand, in models with peak LAI values, around $6 \text{ m}^2 \text{ m}^{-2}$, such as LPJ-GUESS and LPJmL, the estimated GPP was around 50% lower than in the other ones.
Differences in evaporation among DGVMs	INLAND is very sensitive to radiation (Figure S4 in Supporting Information S1). Because of overestimated LAI and SAI, INLAND absorbs high rates of radiation which also contributes to increased evaporation. Moreover, larger LAI means higher transpiration rates, greater rainfall interception, with consequent greater water availability. Transpiration is dependent on LAI (Equation S4 in Supporting Information S1). Another contributing factor is the low root evaporation rates estimated by the LPJmL4 version used in this experiment (Sakschewski et al., 2020). Yet, mechanisms that drive evaporation mainly during the dry season and in more seasonal climates are still poorly understood (Sörensson & Ruscica, 2018).
Differences in WUE among DGVMs	WUE results are not very consistent because WUE is a rate: WUE = GPP/ET. So, WUE is nothing more than the reflection of GPP and ET which are overestimated in some DGVMs and underestimated in others.

the FLUXNET reference data, while LPJmL4 results (the model version that does not include the root strategy) showed underestimated values.

Using the same DGVMs and simulations that we used here, but applied in southern South America, Ruscica et al. (2021) also found a significant trend of decreasing evaporation in the upper La Plata Basin in the summer season. Their results suggest that the trend was due to LUC, as this region has undergone an intense conversion of forests to grasslands.

WUE values were higher in the rainy season. In principle, WUE does not seem to be relevant, given the abundance of water in the Amazon biome. However, several studies have pointed out that there is already a reduction in precipitation, water recycling, and moisture transport as well as an increase in vapor pressure deficit which can aggravate in a scenario of strong anthropogenic impact (Barkhordarian et al., 2019; Davidson et al., 2012; Langenbrunner et al., 2019; Sampaio et al., 2021; Zeng et al., 2008). The difference in WUE values among DGVMs is nothing more than the reflection of differences in GPP and E, which are overestimated in some DGVMs and underestimated in others. Since WUE is a rate: WUE = GPP/E, its results are not very consistent. Some of the discrepancies among DGVMs related to the estimation of GPP, evaporation, and WUE, are summed up in Table 3.

4.3. Climate Changes in the Southern Amazon

We believe that the observed climate changes (increased air temperature, increased radiation, decreased humidity, and precipitation) may be associated with LUC, because the subregion that comprises the south of the state of Pará and part of the northern state of Mato Grosso, Brazil (51°–56°W, 7.5°–12°S), is the one that suffered the greatest deforestation and impacts in the last 30 yr (Aguiar et al., 2007; Lapola et al., 2014; Leite-Filho et al., 2019; Marengo et al., 2018). The changes were more expressive in the dry season, and we observed a good correlation between the increase in temperature, the increase in radiation, and the decrease in specific humidity for this sub-region (Figures 10a, 10c, 10g) which is precisely the region that suffered the longest period of deforestation (Aguiar et al., 2007; Leite-Filho et al., 2019; Ometto, Aguiar, & Martinelli et al., 2014).

In the ensemble of the forcing data, we found an increase in air temperature of up to 1°C in the dry season and 0.6°C in the rainy season in the regions of greatest deforestation. These results are relatively compatible with other observational studies that showed an average temperature increase of 0.6°C for the Amazon from 1973 to 2013 (Almeida et al., 2017; Marengo et al., 2018). Furthermore, L. M. Alves (2016) detected a statistically significant negative rainfall trend in southern Amazonia during the pre-rainy season and the peak of the rainy season during 1979–2014. In addition, Espinoza et al. (2013) showed that while southern Amazonia exhibits negative trends in total rainfall and extremes, the opposite is observed in northern Amazonia.

The decrease in precipitation can be due to natural climate variability. A warming of approximately 0.5°C was observed in the Tropical North Atlantic (L. M. Alves et al., 2012; Trenberth & Shea, 2006), and may have contributed to the occurrence of droughts in the Amazon. Zeng et al. (2008) attribute the origin of decreased precipitation in the Amazon to the Tropical North Atlantic, where precipitation above normal occurs over the ocean, as a typical response of atmospheric convection to the increase in sea surface temperature. This occurs in a Hadley cell, the upward movement of circulation in the north generates subsidence in the south over the Amazon and in the South Atlantic Ocean, which could partly explain the decrease in precipitation that was observed. The results obtained for the sub-region comprising part of Bolivia were different from the rest. In addition to forests, this sub-region comprises *chacos*, *cerrado*, wetlands, and savannas (Tejada et al., 2016).

5. Conclusions

The results show that, in general, the influence of CO_2 fertilization on GPP was greater by an order of magnitude than LUC. In other words, this work shows that the increase of GPP due to CO_2 fertilization was much higher than the losses due to LUC. LUC also had a negative effect on evaporation. The analysis of DGVM results and the forcings showed that the most intense evidence of climate change such as decreased evaporation, temperature increase, and decreased precipitation were seen in the regions that suffered greater deforestation. DGVM results also showed significant divergences among validation data sets. Divergences occur in climate forcings and model internal processes to estimate GPP and evaporation (as discussed in the manuscript), so we think that the results may have been affected in the accuracy of the representation of what actually happens in our study focus biome. This reinforces the need to improve DGVMs and climate data acquisition methods so that more robust simulations can be made on important issues such as the resilience of the Amazon rainforest concerning vegetation GPP, carbon sink, and evaporation in a climate change scenario.

Data Availability Statement

Data from these simulations is available from Zenodo provider—doi.10.5281/zenodo.6374202 and link: https://doi.org/10.5281/zenodo.6374203.

References

Abatzoglou, J. T., Dobrowski, S. Z., Parks, S. A., & Hegewisch, K. C. (2018). TerraClimate, a high-resolution global data set of monthly climate and climatic water balance from 1958–2015. *Scientific Data*, *5*(1), 170191. https://doi.org/10.1038/sdata.2018.191

Aguiar, A. P. D., Camara, G., & Escada, M. (2007). Spatial statistical analysis of land use determinants in the Brazilian Amazonia: Exploring intra-regional heterogeneity. *Ecological Modeling*, *209*, 169–188. https://doi.org/10.1016/j.ecolmodel.2007.06.019

Aguiar, A. P. D., Vieira, I. C. G., Assis, T. O., Dalla-Nora, E. L., Toledo, P. M., Santos-Junior, R. A. O., et al. (2016). Land use change emission scenarios: Anticipating a forest transition process in the Brazilian Amazon. *Global Change Biology*, *22*, 1821–1840. https://doi.org/10.1111/gcb.13134

Ahlström, A., Canadell, J. G., Guy, S., Wu, M., Berry, J. A., Guan, K.,& Jackson, R. B. (2017). Hydrologic resilience and Amazon productivity. *Nature Communications*, *8*, 387. https://doi.org/10.1038/s41467-017-00306-z.2017

Almeida, C. T., Oliveira-Júnior, J. F., Delgado, R. C., Cubo, P., & Ramos, M. C. (2017). Spatio temporal rainfall and temperature trends throughout the Brazilian Legal Amazon, 1973–2013. *International Journal of Climatology*, *37*, 2013–2026. https://doi.org/10.1002/joc.4831

Alves, D. S. (2002). Space-time dynamics of deforestation in Brazilian Amazônia. *International Journal of Remote Sensing*, *23*(14), 2903–2908. https://doi.org/10.1080/01431160110096791

Alves, L. M. (2016). *Análise estatística da sazonalidade e tendências das estações chuvosas e seca na Amazônia: Clima presente e projeções futuras, (Ph.D. thesis)*. Instituto Nacional de Pesquisas Espaciais, São José dos Campos.

Alves, L. M., Marengo, J. A., & Cavalcanti, I. F. A. (2012). *Histórico de Secas na Amazônia*. Retrieved from https://www.researchgate.net/publication/322131862_Historico_de_Secas_na_Amazonia

Arora, V. K., & Boer, G. J. (2005). Fire as an interactive component of dynamic vegetation models. *Journal of Geophysical Research*, *110*, G02008. https://doi.org/10.1029/2005JG000042

Avissar, R., Silva Dias, P. L., Silva Dias, M. A. F., & Nobre, C. (2002). The Large-Scale Biosphere-Atmosphere Experiment in Amazonia (LBA): Insights and future research needs. *Journal of Geophysical Research*, *107*(D20), 8086. https://doi.org/10.1029/2002JD002704

Azevedo, A. A., Rajão, R., Costa, M. A., Stabile, M. C. C., Macedo, M. N., dos Reis, T. N. P., et al. (2017). Limits of Brazil's Forest Code as a means to end illegal deforestation. *Proceedings of the National Academy of Sciences of the United States of America*, *114*, 7653–7658. https://doi.org/10.1073/pnas.1604768114

Baldocchi, D., Falge, E., Gu, L., Olson, R., Hollinger, D., Running, S., et al. (2001). FLUXNET: A new tool to study the temporal and spatial variability of ecosystem-scale carbon dioxide, water vapor, and energy flux densities. *Cover Bulletin of the American Meteorological Society Bulletin of the American Meteorological Society*, 2415–2434. https://doi.org/10.1175/1520-0477(2001)082<2415:fantts>2.3.co;2

Ball, J. T., Woodrow, I. E., & Berry, J. A. (1987). A model predicting stomatal conductance and its to the control of photosynthesis under different environmental conditions. In I.Biggins (Ed.), *Progress in photosynthesis* (pp. 221–224). Martinus Nijhoff Publishers. https://doi.org/10.1007/978-94-017-0519-6_48

Barkhordarian, A., Saatchi, S. S., Behrangi, A., Loikith, P. C., & Mechoso, C. R. (2019). A recent systematic increase in vapor pressure deficit over tropical South America. *Scientific Reports*, *9*(1), 15331. https://doi.org/10.1038/s41598-019-51857-8

Barlow, J., Franca, F., Gardner, T. A., Hicks, C. C., Lennox, G. D., Berenguer, E., et al. (2018). The future of hyperdiverse tropical ecosystems. *Nature*, *559*, 517–526. https://doi.org/10.1038/s41586-018-0301-1

Barlow, J., Gardner, T. A., Araujo, I. S., Ávila-Pires, T. C., Bonaldo, A. B., Costa, J. E., et al. (2007). Quantifying the biodiversity value of tropical primary, secondary, and plantation forests. *Proceedings of the National Academy of Sciences of the United States of America*, *104*, 18555–18560. https://doi.org/10.1073/pnas.0703333104

Barlow, J., Lennox, G. D., Ferreira, J., Berenguer, E., Lees, A. C., Mac Nally, R., et al. (2016). Anthropogenic disturbance in tropical forests can double biodiversity loss from deforestation. *Nature*, *535*, 144–147. https://doi.org/10.1038/nature18326

Bonan, G. B., Oleson, K. W., Fisher, R. A., Lasslop, G., & Reichstein, M. (2012). Reconciling leaf physiological traits and canopy flux data use of the TRY and FLUXNET databases in the Community Land Model version 4. *Journal of Geophysical Research*, *117*(25C), 1–19. https://doi.org/10.1029/2011JG001913

Brienen, R. J. W., Phillips, O. L., Feldpausch, T. R., Gloor, E., Baker, T. R., Lloyd, J., et al. (2015). Long-term decline of the Amazon carbon sink. *Nature*, *519*(7543), 344–348.

Cardille, J. A., & Foley, J. A. (2003). Agricultural land use change in Brazilian Amazonia between 1980 and 1995: Evidence from integrated satellite and census data. *Remote Sensing of Environment*, *87*, 551–562. https://doi.org/10.1016/j.rse.2002.09.001

Chiarutti, A., Araújo, M. B., Decocq, G., Beierkuhnlein, C., & Fernández-Palacios, J. M. (2010). The concept of potential natural vegetation: An epitaph? *Journal of Vegetation Science*, *21*, 1172–1178. https://doi.org/10.1111/j.1654-1103.2010.01218.x

Collatz, G. J., Ball, J. T., Griveta, C., & Berrya, J. A. (1991). Physiological and environmental regulation of stomatal conductance, photosynthesis, and transpiration: A model that includes a laminar boundary layer. *Agricultural and Forest Meteorology*, *54*, 107–136. https://doi.org/10.1016/0168-1923(91)90002-8

Collatz, G. J., Ribas-Carbo, M., & Berry, J. A. (1992). Coupled photosynthesis-stomatal conductance model for leaves of C_4 plants. *Australian Journal of Plant Physiology*, *19*, 519–538. https://doi.org/10.1071/pp9920519

Cuartas, L. A., Tomasella, J., Nobre, A. D., Hodnett, M. G., Waterloo, M. J., & Munera, J. C. (2007). Interception water-partitioning dynamics for a pristine rainforest in central Amazonia: Marked differences between normal and dry years. *Agricultural and Forest Meteorology*, *145*, 69–83. https://doi.org/10.1016/j.agrformet.2007.04.008

Czikowsky, M. J., & Fitzjarrald, D. R. (2009). Detecting rainfall interception in an Amazonian rain forest with eddy flux measurements. *Journal of Hydrology*, *377*, 92–105. https://doi.org/10.1016/j.jhydrol.2009.08.002

Davidson, E., de Araújo, A. A. C., Artaxo, P., Balch, J. K., Brown, I. F., Mercedes, M., et al. (2012). The Amazon basin in transition. *Nature*, *481*, 321–328. https://doi.org/10.1038/nature10717

De Kauwe, M. G., Lin, Y.-S., Wright, I. J., Medlyn, B. E., Crous, K. Y., Ellsworth, D. S., et al. (2015). A test of the "one-point method" for estimating maximum carboxylation capacity from field-measured, light-saturated photosynthesis. *New Phytologist*, *210*(3), 1130–1144. https://doi.org/10.1111/nph.13815

Dias, L.C.P., Pimenta, F. M., Santos, A. B., Costa, M. H., & Ladle, R. J. (2016). Patterns of land use, extensification and intensification of Brazilian agriculture. *Global Change Biology*, *22*, 2887–2903. https://doi.org/10.1111/gcb.13314

Dietze, M. C. (2014). Gaps in knowledge and data driving uncertainty in models of photosynthesis. *Photosynthesis Research*, *119*, 3–14. https://doi.org/10.1007/s11120-013-9836-z

Dirmeyer, P. A., Schlosser, C. A., & Brubaker, K. L. (2009). Precipitation, recycling, and land memory: An integrated analysis. *Journal of Hydrometeorology*, *1*, 278–288. https://doi.org/10.1175/2008JHM1016.1

Dolman, A. J., & Janssen, T. A. J. (2018). The enigma of the Amazonian carbon balance. *Environmental Research Letters*, *13*, 061002 https://doi.org/10.1088/1748-9326/aac78e

Espinoza, J. C., Josyane, R., Frédéric, F., Waldo, L., William, S., & Jean Loup, G. (2013). The major floods in the Amazonas river and tributaries (Western Amazon basin) during the 1970–2012 period: A focus on the 2012 flood. *Journal of Hydrometeorology*, *14*, 1000–1008. https://doi.org/10.1175/JHM-D-12-0100.1

Farquhar, G. D., von Caemmerer, S., & Berry, J. A. (1980). A biochemical model of photosynthetic CO_2 assimilation in leaves of C_3 species. *Planta*, *149*, 78–90. https://doi.org/10.1007/bf00386231

Foley, J. A., Prentice, I. C., Ramankutty, N., Levis, S., Pollard, D., Sitch, S., & Haxeltine, A. (1996). An integrated biosphere model of land surface processes, terrestrial carbon balance, and vegetation dynamics. *Global Biogeochemical Cycles*, *10*(4), 603–628. https://doi.org/10.1029/96gb02692

Fleischer, K., Rammig, A., De Kauwe, M. G., Walker, A. P., Domingues, T. F., Fuchslueger, L., et al. (2019). Amazon forest response to CO_2 fertilization dependent on plant phosphorus acquisition. *Nature Geoscience*, *12*, 736–741. https://doi.org/10.1038/s41561-019-0404-9

Gatti, L., Baso, L. S., Miller, J. B., Gloor, M., Domingues, L. G., Cassol, H. L. G., et al. (2021). Amazonia as a carbon source linked to deforestation and climate change. *Nature Volume*, *595*, 388–393.

Harper, A., Baker, I. T., Denning, A. S., Randall, D. A., Dazlich, D., & Branson, M. (2014). Impact of evapotranspiration on dry season climate in the Amazon forest. *Journal of Climate*, 574–591. https://doi.org/10.1175/JCLI-D-13-00074.1

Hickler, T., Vohland, K., Feehan, J., Miller, P. A., Smith, B., Costa, L., et al. (2012). Projecting the future distribution of European potential natural vegetation zones with a generalized, tree species based dynamic vegetation model. *Global Ecology Biogeography*, *21*, 50–63. https://doi.org/10.1111/j.1466-8238.2010.00613.x

Hubau, W., Lewis, S. L., Phillips, O. L., Affum-Baffoe, K., Beeckman, H., Cuní-Sanchez, A., et al. (2020). Asynchronous carbon sink saturation in African and Amazonian tropical forests. *Nature*, *579*, 80–87.

Hurtt, G. C., Chini, L., Sahajpal, R., Frolking, S., Bodirsky, B. L., Calvin, K., et al. (2020). Harmonization of global land use change and management for the period 850–2100 (LUH2) for CMIP6. *Geoscientific Model Development*, *13*, 5425–5464. https://doi.org/10.5194/gmd-13-5425-2020

INPE. (2020). *PRODES—Monitoramento da Floresta Amazônica Brazileira por Satélite*. [WWW Document]. Instituto Nacional de Pesquisas Espaciais website. Retrieved 30 September 2020 from http://www.obt.inpe.br/OBT/assuntos/programas/amazonia/prodes

Intergovernmental Panel on Climate Change (IPCC). (2019). *Chapter 4—Land degradation*.

Jung, M., Schwalm, C., Migliavacca, M., Walther, S., Camps-Valls, G., Koirala, S., et al. (2020). Scaling carbon fluxes from eddy covariance sites to globe: Synthesis and evaluation of the FLUXCOM approach. *Biogeosciences*, *17*, 1343–1365. https://doi.org/10.5194/bg-17-1343-2020

Kalamandeen, M., Gloor, E., Mitchard, E., Quincey, D., Ziv, G., Spracklen, D., et al. (2018). Pervasive rise of small-scale deforestation in Amazonia. *Scientific Reports*, *8*, 1600. https://doi.org/10.1038/s41598-018-19358-2

Kileen, T. J., Calderon, V., Soria, L., Quezada, B., Steininger, M. K., Harper, G., et al. (2007). Thirty years of land-cover change in Bolivia. *AMBIO: A Journal of the Human Environment*, *36*(7), 600–606. https://doi.org/10.1579/0044-7447

Kim, H. (2017). Global Soil Wetness Project Phase 3 Atmospheric Boundary Conditions (Experiment 1). [Dataset]. Data Integration and Analysis System (DIAS). https://doi.org/10.20783/DIAS.501

Krinner, G., Viovy, N., de Noblet-Ducoudré, N., Ogée, J., Polcher, J., Friedlingstein, P., et al. (2005). A dynamic global vegetation model for studies of the coupled atmosphere-biosphere system. *Global Biogeochemical Cycles*, *19*, GB1015. https://doi.org/10.1029/2003GB002199

Kucharik, C. J., Foley, J. A., Delire, C., Fisher, V. A., Coe, M. T., Lenters, J. D., et al. (2000). Testing the performance of a dynamic global ecosystem model: Water balance, carbon balance, and vegetation structure. *Global Biogeochemical Cycles*, *14*(3), 795–825. https://doi.org/10.1029/1999gb001138

Langenbrunner, B., Pritchard, M. S., Kooperman, G. J., & Randerson, J. T. (2019). Why does Amazon precipitation decrease when tropical forests respond to increasing CO_2? *Earth's Future*, *7*(4), 450–468. https://doi.org/10.1029/2018EF001026

Lapola, D. M., Martinelli, L. A., Peres, C. A., Ometto, J. P. H. B., Ferreira, M. E., Nobre, C. A., et al. (2014). Pervasive transition of the Brazilian land use system. *Nature Climate Change*, *4*. https://doi.org/10.1038/NCLIMATE2056

Lebauer, D. S., Wang, D., Richter, K. T., Davidson, C. C., & Dietze, M. C.(2013). Facilitating feedbacks between field measurements and ecosystem models. *Ecological Monographs*, *83*(2), 133–154.

Leipprand, A., & Gerten, D. (2006). Global effects of doubled atmospheric CO_2 content on evapotranspiration, soil moisture, and runoff under potential natural vegetation. *Hydrological Sciences Journal*, 171–185. ISSN: 0262-6667 (Print) 2150-3435.

Leite, C. C., Costa, M. H., de Lima, C. A., Ribeiro, C. A. A. S., & Sediyama, G. C. (2011). Historical reconstruction of land use in Brazilian Amazon (1940–1995). *Journal of Land Use Science*, *6*, 33–52. https://doi.org/10.1080/1747423X.2010.501157

Leite-Filho, A. T., Costa, M. H., & Fu, R. (2019). The southern Amazon rainy season: The role of deforestation and its interactions with large-scale mechanisms. *International Journal of Climatology*, *40*(4), 2328–2341. https://doi.org/10.1002/joc.6335

Leuning, R. (1995). A critical appraisal of a combined stomatal photosynthesis model for C_3 plants. *Plant, Cell and Environment*, *18*, 339–355. https://doi.org/10.1111/j.1365-3040.1995.tb00370.x

Li, W. H., & Fu, R. (2004). Transition of large-scale atmospheric and land surface conditions from the dry to the wet season over Amazonia as diagnosed by the ECMWF reanalysis. *Journal of Climate*, *17*, 2637–2651. https://doi.org/10.1175/1520-0442(2004)017<2637:TOTLAA>2.0.CO;2

Llopart, M., Reboita, M. S., Coppola, E., Giorgi, F., Da Rocha, R. P., & De Souza, D. O. (2018). Land use change over the Amazon forest and its impact on the local climate. *Water*, *10*, 149. https://doi.org/10.3390/w10020149

Madani, N., & Parazoo, N.C. (2020). *Global Monthly GPP from an Improved Light Use Efficiency Model, 1982-2016*. ORNL DAAC. https://doi.org/10.3334/ORNLDAAC/1789

Marengo, J. A., Souza, C. M., Thonicke, K., Burton, C., Halladay, K., Betts, R. A., et al. (2018). Changes in climate and land use over the Amazon region: Current and future variability and trends. *Frontiers in Earth Science*, *6*, 228. https://doi.org/10.3389/feart.2018.00228

Martens, B., Miralles, D. G., Lievens, H., Fernández-Prieto, D., & Verhoest, N. E. C. (2016). Improving terrestrial evaporation estimates over continental Australia through assimilation of SMOS soil moisture. *International Journal of Applied Earth Observations and Geoinformation*, *48*, 146–162. https://doi.org/10.1016/j.jag.2015.09.012

Martens, B., Miralles, D. G., Lievens, H., van der Schalie, R., de Jeu, R. A. M., Fernández-Prieto, D., et al. (2017). GLEAM v3: Satellite-based land evaporation and root-zone soil moisture. *Geoscientific Model Development*, *10*, 1903–1925.

Miralles, D. G., Brutsaert, W., Dolman, A. J., & Gash, J. H. (2020). On the use of the term "evapotranspiration". *Water Resources Research*, *56*(11), e2020WR028055. https://doi.org/10.1029/2020WR028055

Miralles, D. G., de Jeu, R. A. M., Gash, J. H., Holmes, T. R. H., & Dolman, A. J. (2011). Magnitude and variability of land evaporation and its components at the global scale. *Hydrology and Earth System Sciences*, *15*, 967–981. https://doi.org/10.5194/hess-15-967-2011

Miralles, D. G., Gash, J. H., Holmes, T. R. H., de Jeu, R. A. M., & Dolman, A. J. (2010). Global canopy interception from satellite observations. *Journal of Geophysical Research*, *115*, D16122. https://doi.org/10.1029/2009jd013530

Miralles, D. G., Holmes, T. R. H., de Jeu, R. A. M., Gash, J. H., Meesters, A. G. C. A., & Dolman, A. J. (2011). Global land-surface evaporation estimated from satellite-based observations. *Hydrology and Earth System Sciences*, *15*, 453–469. https://doi.org/10.5194/hess-15-453-2011

Moffat, A. M., Papale, D., Reichstein, M., Hollinger, D. Y., Richardson, A. D., Barr, A. G., et al. (2007). Comprehensive comparison of gap-filling techniques for eddy covariance net carbon fluxes. *Agricultural and Forest Meteorology*, *147*, 209–232. https://doi.org/10.1016/j.agrformet.2007.08.011

Muller-Hansen, F., Cardoso, M. F., Dalla-Nora, E. L., Donges, J. F., Heitzig, J., Kurths, J., & Thonicke, K. (2017). A matrix clustering method to explore patterns of land-cover transitions in satellite-derived maps of the Brazilian Amazon. *Nonlinear Processes in Geophysics*, *24*, 113–123. https://doi.org/10.5194/npg-24-113-2017

Nepstad, D., Mcgrath, D., Stickler, C., Alencar, A., Azevedo, A., Swette, B., et al. (2014). Slowing Amazon deforestation through public policy and interventions in beef and soy supply chains. *Science*, *344*, 1118–1123. https://doi.org/10.1126/science.1248525

Nobre, C. A., Sellers, P. J., Shukla, J. (1991). Amazonian deforestation and regional climate change. *Journal of Climate*, *4*, 957–988. https://doi.org/10.1175/1520-0442(1991)004<0957:ADARCC>2.0.CO;2

Norby, J. R., De Kauwe, M. G., Domingues, T. F., Duursma, R. A., Ellsworth, D. S., Goll, D. S., et al. (2015). Model-data synthesis for the next generation of forest free-air CO_2 enrichment (FACE) experiments. *New Phytologist*, *209*(1), 17–28. https://doi.org/10.1111/nph.13593

Ometto, J. P., Aguiar, A. P. D., Assis, T., Soler, L., Valle, P., Tejada, G., et al. (2014). Amazon forest biomass density maps: Tackling the uncertainty in carbon emission estimates. *Climatic Change*, *124*, 545–560. https://doi.org/10.1007/s10584-014-1058-7

Ometto, J. P., Aguiar, A. P. D., & Martinelli, L. A. (2014). Amazon deforestation in Brazil: Effects, drivers and challenges. *Carbon Management*, *2*(5), 575–585. https://doi.org/10.4155/cmt.11.48

Pan, Y., Birdsey, R. A., Fang, J., Houghton, R., Kauppi, P. E., Kurz, W. A., et al. (2011). A large and persistent carbon sink in the world's forests. *Science*, *333*, 988–993. https://doi.org/10.1126/science.1201609

Papale, D., Reichstein, M., Aubinet, M., Canfora, E., Bernhofer, C., Kutsch, W., et al. (2006). Towards a standardized processing of net ecosystem exchange measured with eddy covariance technique: Algorithms and uncertainty estimation. *Biogeosciences*, *3*, 571–583. https://doi.org/10.5194/bg-3-571-2006

Phillips, O. L., & Roel, J. W. (2017). Brienen and the RAINFOR collaboration. Carbon uptake by mature Amazon forests has mitigated Amazon nations' carbon emissions. *Carbon Balance Manage*, *12*, 1. https://doi.org/10.1186/s13021-016-0069-2

Prentice, I. C., Bondeau, A., Cramer, W., Harrison, S. P., Hickler, T., Lucht, W., et al. (2007). Dynamic global vegetation modeling: Quantifying terrestrial ecosystem responses to large-scale environmental change. In J.Canadell, D.Pataki, & L.Pitelka (Eds.), *Terrestrial ecosystems in a changing world*. Springer.

Quillet, A., Peng, C., & Garneau, M. (2009). Toward dynamic global vegetation models for simulating vegetation-climate interactions and feedbacks: Recent developments, limitations, and future challenges. *Environmental Reviews*, *18*, 333–353. https://doi.org/10.1139/A10-016

Reichstein, M., Falge, E., Baldocchi, D., Papale, D., Aubinet, M., Berbigier, P., et al. (2005). On the separation of net ecosystem exchange into assimilation and ecosystem respiration: Review and improved algorithm. *Global Change Biology*, *11*, 1424–1439. https://doi.org/10.1111/j.1365-2486.2005.001002.x

Restrepo-Coupea, N., da Rocha, H. R., Hutyra, L. R., da Araujo, A. C., Borma, L. S., Christoffersen, B., et al. (2013). What drives the seasonality of photosynthesis across the Amazon basin? A cross-site analysis of eddy flux tower measurements from the Brazil flux network. *Agricultural and Forest Meteorology*, *182–183*, 128–144. https://doi.org/10.1016/j.agrformet.2013.04.031

Rezende, L. F. C., Arenque, B. C., Aidar, S. T., Moura, M. S. B., Von Randow, C., Tourigny, E., et al. (2015). Evolution and challenges of dynamic global vegetation models for some aspects of plant physiology and elevated atmospheric CO_2. *International Journal of Biometeorology*, *60*(7), 945–955. https://doi.org/10.1007/s00484-015-1087-6

Rodell, M., Houser, P. R., Jambor, U., Gottschalck, J., Mitchell, K., Meng, C.-J., et al. (2004). The global land data assimilation system. *Bulletin of the American Meteorological Society*, *85*(3), 381–394. https://doi.org/10.1175/bams-85-3-381

Rogers, A. (2014). The use and misuse of Vc_{max} in Earth system models. *Photosynthesis Research*, *119*, 15–29. https://doi.org/10.1007/s11120-013-9818-1

Ruscica, R.C., Sörensson, A. A., Diaz, L. B., Vera, C., Castro, A., Papastefanou, P., et al. (2021). Evapotranspiration trends and variability in southeastern South America: The roles of land-cover change and precipitation variability. *International Journal of Climatology*. Accepted AuthorManuscript. https://doi.org/10.1002/joc.7350

Ryu, Y., Berry, J. A., & Baldocchi, D. D. (2019). What is global photosynthesis? History, uncertainties, and opportunities. *Remote Sensing of Environment*, *223*, 95–114. https://doi.org/10.1016/j.rse.2019.01.016

Sakschewski, B., von Bloh, W., Druke, M., Sorensson, A. A., et al. (2020). Variable tree rooting strategies improve tropical productivity and evapotranspiration in a dynamic global vegetation model. *Biogeosciences Discussions*. Preprint. Discussion started: 27 March 2020. https://doi.org/10.5194/bg-2020-97

Sampaio, G., Nobre, C., Costa, M. H., Satyamurty, P., Soares-Filho, B. S., Cardoso, M., et al. (2007). Regional climate change over eastern Amazonia caused by pasture and soybean cropland expansion. *Geophysical Research Letters*, *34*, L17709, https://doi.org/10.1029/2007GL030612

Sampaio, G., Shimizu, M., Carlos, A., Guimarães-Júnior, Alexandre, F., Cardoso, M., et al. (2021). CO_2 physiological effect can cause rainfall decrease as strong as large-scale deforestation in the Amazon. *Biogeosciences*, *18*, 2511–2525. https://doi.org/10.5194/bg-18-2511-2021

Schaphoff, S., von Bloh, W., Rammig, A., Thonicke, K., Biemans, H., Forkel, M., et al. (2018). LPJmL4—A dynamic global vegetation model with managed land—Part 1: Model description. *Geoscientific Model Development*, *11*, 1343–1375. https://doi.org/10.5194/gmd-11-1343-2018

Scheiter, S., Langan, L., & Higgins, S. I. (2013). Next-generation dynamic global vegetation models: Learning from community ecology. *New Phytologist*, *198*, 957–969. https://doi.org/10.1111/nph.12210

Schimel, D., Pavlick, R., Fisher, J. B., Asner, G. P., Saatchi, S., Townsend, P., et al. (2015). Observing terrestrial ecosystems and the carbon cycle from space. *Global Change Biology*, *21*, 1762–1776. https://doi.org/10.1111/gcb.12822

Silva Dias, M. A. F., Rutledge, S., Kabat, P., Silva Dias, P. L., Nobre, C., Fisch, G., et al. (2002). Cloud and rain processes in a biosphere-atmosphere interaction context in the Amazon Region. *Journal of Geophysical Research*, *107*(D20), 8072, https://doi.org/10.1029/2001JD000335

Sitch, S., Smith, B., Prentice, I. C., Arneth, A., Bondeau, A., Cramer, W., et al. (2003). Evaluation of ecosystem dynamics, plant geography, and terrestrial carbon cycling in the LPJ dynamic global vegetation model. *Global Change Biology*, *9*(2), 161–185. https://doi.org/10.1046/j.1365-2486.2003.00569.x

Smith, B. (2001). Representation of vegetation dynamics in the modelling of terrestrial ecosystems: Comparing two contrasting approaches within European climate space. *Global Ecology and Biogeography*, *10*, 621–637. https://doi.org/10.1046/j.1466-822x.2001.00256.x

Smith, N. G., & Dukes, J. S. (2012). Plant respiration and photosynthesis in global-scale models: Incorporating acclimation to temperature and CO_2. *Global Change Biology*. https://doi.org/10.1111/j.1365-2486.2012.02797.x.2012

Sörensson, A. A., & Ruscica, R. C. (2018). Intercomparison and uncertainty assessment of nine evapotranspiration estimates over South America. *Water Resources Research*, *54*(4), 2891–2908. https://doi.org/10.1002/2017WR021682

Tejada, G., Dalla-Nora, E., Cordoba, D., Lafortezza, R., Ovando, A., Assis, T., et al. (2016). Deforestation scenarios for Bolivian lowlands. *Environmental Research*, *144*, 49–63. https://doi.org/10.1016/j.envres.2015.10.010

Tourigny, E. (2014). *Multi-scale fire modeling in the neotropics: Coupling a land surface model to a high-resolution fire spread model, considering land cover heterogeneity, (Ph.D. dissertation, meteorology)*. INPE. Retrieved from http://urlib.net/sid.inpe.br/mtc-m21b/2014/05.30.00.36

Trenberth, K., & Shea, D. J. (2006). Atlantic hurricanes and natural variability in 2005. *Geophysical Research Letters 33*, L12704, https://doi.org/10.1029/2006gl026894

Ueyama, M., Ichii, K., Kobayashi, H., Kumagai, T., Beringer, J., Merbold, L., et al. (2020). Inferring CO_2 fertilization effect based on global monitoring land-atmosphere exchange with a theoretical model. *Environmental Research Letters*, *15*, 084009 https://doi.org/10.1088/1748-9326/ab79e5

Valentini, R., Arneth, A., Bombelli, A., Castaldi, S., Cazzolla Gatti, R., Chevallier, F., et al. (2014). A full greenhouse gases budget of Africa: Synthesis, uncertainties, and vulnerabilities. *Biogeosciences*, *11*, 381–407. https://doi.org/10.5194/bg-11-381-2014

van der Ent, R. J., Savenije, H. H. G., Schaefli, B., & Steele-Dunne, S. C. (2010). Origin and fate of atmospheric moisture over continents. *Water Resources Research*, *46*, W09525. https://doi.org/10.1029/2010WR009127

Von Randow, C., Kruijt, B., Holtslag, A. A. M., & de Oliveira, M. B. L. (2008). Exploring eddy-covariance and large-aperture scintillometer measurements in an Amazonian rain forest. *Agricultural and Forest Meteorology*, *148*, 680–690. https://doi.org/10.1016/j.agrformet.2007.11.011

Von Randow, C., Manzi, A. O., Kruijt, B., de Oliveira, P. J., Zanchi, F. B., Silva, R. L., et al. (2004). Comparative measurements and seasonal variations in energy and carbon exchange over forest and pasture in South West Amazonia. *Theoretical and Applied Climatology*, *78*, 5–26. https://doi.org/10.1007/s00704-004-0041-z

Von Randow, R. C. S., Tomasella, J., von Randow, C., de Araújo, A. C., Manzi, A. O., Hutjes, R., et al. (2020). Evapotranspiration and gross primary productivity of secondary vegetation in Amazonia inferred by eddy covariance. *Agricultural and Forest Meteorology*, *294*, 108141. https://doi.org/10.1016/j.agrformet.2020.108141

Walker, A. P., De Kauwe, M. G., Bastos, A., Belmecheri, S., Georgioum, K., Keeling, R. F., et al. (2020). Integrating the evidence for a terrestrial carbon sink caused by increasing atmospheric CO_2. *New Phytologist*. https://doi.org/10.1111/nph.16866

Wang, S., Zhang, Y., Ju, W., Chen, J. M., Ciais, P., Cescatti, A., et al. (2020). Recent global decline of CO_2 fertilization effects on vegetation photosynthesis. *Science*, *370*, 1295–1300. https://doi.org/10.1126/science.abb7772

Weedon, G. P., Balsamo, G., Bellouin, N., Gomes, S., Best, M. J., & Viterbo, P. (2014). Data methodology applied to ERA-Interim reanalysis data. *Water Resources Research*, *50*, 7505–7514. https://doi.org/10.1002/2014WR015638.Received

Weedon, G. P., Gomes, S., Viterbo, P., Shuttleworth, W. J., Blyth, E., Österle, H., et al. (2011). Creation of the WATCH forcing data and its use to assess global and regional reference crop evaporation over land during the twentieth century. *Journal of Hydrometeorology*, *12*(5), 823–848. https://doi.org/10.1175/2011jhm1369.1

Wu, M., Schurgers, G., Rummukainen, M., Smith, B., Samuelsson, P., Jansson, C., et al. (2016). Vegetation-climate feedbacks modulate rainfall patterns in Africa under future climate change. *Earth System Dynamics*, *7*, 627–647. https://doi.org/10.5194/esd-7-627-2016

Yi, C., Ricciuto, D., Li, R., Wolbeck, J., Xu, X., Nilsson, M., et al. (2010). Climate control of terrestrial carbon exchange across biomes and continents. *Environmental Research Letters*, *5*, 034007. https://doi.org/10.1088/1748-9326/5/3/034007

Zemp, D. C., Schleussner, C.-F., Barbosa, H. M. J., van der Ent, R. J., Donges, J. F., Heinke, J., et al. (2014). On the importance of cascading moisture recycling in South America. *Atmospheric Chemistry and Physics*, *14*(23), 13337–13359. https://doi.org/10.5194/acp-14-13337-2014

Zeng, N., Yoon, J.-H., Marengo, J. A., Subramaniam, A., Nobre, C. A., Mariott, A., Neelin, J. D. (2008). Causes and impacts of the 2005 Amazon drought. *Environmental Research Letters*, *3*, 014002. https://doi.org/10.1088/1748-9326/3/1/014002